Multi-omics Analyses of Starvation Responses Reveal a Central Role for Lipoprotein Metabolism in Acute Starvation Survival in C. elegans

Harvald, Eva Bang; Sprenger, Richard R.; Dall, Kathrine Brændgaard; Ejsing, Christer S.; Nielsen, Ronni; Mandrup, Susanne

Published in:
Cell Systems

DOI:
10.1016/j.cels.2017.06.004

Publication date:
2017

Global proteomic- and transcriptomic analyses of starvation responses reveal a central role for lipoprotein metabolism in acute starvation survival in *C. elegans*

Eva Bang Harvald[a], Richard R. Sprenger[a], Kathrine Brændgaard Dall[a], Christer S. Ejsing[a], Ronni Nielsen[a], Susanne Mandrup[a], Anton Gartner[b], Angus I. Lamond[b], Nils J. Færgeman[a§]

[a]Villum Center for Bioanalytical Sciences, Department of Biochemistry and Molecular Biology, University of Southern Denmark, DK-5230 Odense M, Denmark

[b]Centre for Gene Regulation and Expression, College of Life Science, University of Dundee, Dow St, Dundee, United Kingdom, DD15EH

[§]Lead contact: Nils J. Færgeman, Villum Center for Bioanalytical Sciences, Department of Biochemistry and Molecular Biology, University of Southern Denmark, DK-5230 Odense M, Denmark, Tel. +45 6550 2453; Fax. +45 6550 2467; E-mail: nils.f@bmb.sdu.dk

Keywords: *C. elegans*, starvation, HLH-30, proteomics, transcriptomics, RNA-seq, vitellogenins, lipid droplets

Abbreviations:

ATG, AuTophagy Gene; CARS, Coherent Anti-stokes Raman Scattering; GO term, Gene Ontology term; KEGG, Kyoto Encyclopedia of Genes and Genomes; LC-MS, Liquid Chromatography-Mass Spectrometry; MS, Mass Spectrometry; NGM, Nematode Growth Media; RNA-seq, RNA-sequencing; SILAC, Stable Isotope Labeling by Amino acids in Cell culture

SUMMARY

Despite the fact that mild starvation is known to have beneficial effects on organisms ranging from yeast to primates, the molecular mechanisms underlying the physiological and cellular response to starvation have by far been fully resolved. In the present study we have used 2D-LC-MS label-free quantitative proteomics and RNA-seq to examine the temporal responses to starvation in the multicellular organism *C. elegans* in both wild type animals and *hlh-30* mutants. HLH-30, a homolog of the mammalian transcription factor TFEB, is known to serve important functions in the response and adaptation to starvation. Our proteomic analysis identified more than 4,500 proteins at each of the seven time points examined in both wild type and *hlh-30* mutant animals with nearly complete data coverage. By RNA-seq analysis we identified close to ~41,000 annotated RNAs of which more than 20,000 encode a protein product. We found that protein abundance shows a moderate correlation with the abundance of the corresponding mRNAs throughout the starvation period, underlining that protein levels are not predominantly regulated by transcriptional mechanisms. Our findings show that starvation alters the abundance of hundreds of mRNAs and proteins in a temporal manner, which are involved in central metabolic pathways including lipoprotein metabolism. Interestingly, we find that *hlh-30* animals die prematurely under starving condition, which can prevented by knock down of *vit-1* and *vit-5*, encoding specific lipoproteins involved in transport of lipids and other nutrients from the intestine to the oocyte. We also show that the size and number of intestinal lipid droplets are altered in *hlh-30* animals, which is normalized by knock down of *vit-1* and *vit-5*, collectively indicating that the improved survival under starvation conditions is closely linked to the size and number of the intestinal lipid droplets. We conclude that our present study provides an extensive and important resource for further functional studies of starvation responses in *C. elegans*.

INTRODUCTION

A fundamental challenge for all living organisms is to sense and respond to nutrient-derived signals in order to adapt their metabolism and physiology to promote survival and achieve balanced growth. Accordingly, evolution has shaped the ability of organisms to regulate its metabolism in response to nutrient availability. Thus, by coordinating catabolic as well as anabolic pathways, organisms from yeast and bacteria to humans are capable of survival with extended minimum energy intake. Interestingly, several studies have shown that either reduced caloric intake or fasting periods without malnutrition, can have numerous beneficial effects including enhanced cognitive functions and improved immune responses, reduced risk of developing metabolic and neurodegenerative diseases, and even improved treatment of certain types of cancers (reviewed in (Longo and Mattson, 2014)). During the past decades many studies have uncovered mechanisms governing regulation and adaptation to starvation, including controlled depletion of energy stores to sustain a nutrient limited environment. In particular, lipolysis (Narbonne and Roy, 2009; O'Rourke and Ruvkun, 2013), lipophagy (reviewed in (Liu and Czaja, 2013)) and subsequently breakdown of fatty acids through β-oxidation (Elle et al., 2012; Settembre et al., 2013) have been shown to be important for survival during starvation.

The helix-loop-helix transcription factor HLH-30 in *C. elegans* and its mammalian orthologue, TFEB, have previously been shown to serve a central role in starvation responses by coordinating the induction of genes involved in autophagosome formation, lysosomal functions, and fatty acid degradation, thus preventing accumulation of potentially harmful intermediates (Cuervo, 2013; Lapierre et al., 2013; O'Rourke and Ruvkun, 2013; Pena-Llopis et al., 2011). Accordingly, impaired HLH-30 function does not affect lifespan under normal conditions, but compromises the long-lived phenotype of multiple *C. elegans* mutants including *eat-2* (dietary restriction), *glp-1* (impaired fertility), *daf-2* (insulin signaling), *clk-1* (respiration), *rsks-1* (translation), *mlx-3* (increased lipid degradation), and the RNAi depletion of the TOR orthologue *let-363* (Lapierre et al., 2013). Moreover, *hlh-30* mutants die prematurely during starvation (O'Rourke and Ruvkun, 2013),

underlining the importance of HLH-30 for the physiological response to starvation. Additionally, HLH-30 is also required for antimicrobial responses (Visvikis et al., 2014). Collectively, these studies show that HLH-30 serves multiple functions and imply that it may also control still unrevealed pathways.

Despite the previous studies, the underlying mechanisms regulating the delicate balance between energy consumption and energy storage have not been fully investigated and our current knowledge is limited by a prevalent focus on single pathways such as lipid catabolism (O'Rourke and Ruvkun, 2013), autophagy (Kang et al., 2007), and translation (Hansen et al., 2007) rather than a systematic, global analysis of how all pathways are wired and interconnected. While control of starvation has been studied in details at a genetic level, relatively little is known about how the proteome change in response to starvation. Recent developments in quantitative proteomics in *C. elegans* have provided further opportunities to systematically examine proteomic changes in response to environmental and genetic changes (Fredens et al., 2011; Larance et al., 2011) and aging (Dong et al., 2007; Liang et al., 2014; Narayan et al., 2016; Walther et al., 2015; Zimmerman et al., 2015). Importantly, these and other studies have also revealed that there is only a modest correlation between mRNA and proteins levels (Grun et al., 2014; Walther et al., 2015) elevating the importance of determining information on both levels of regulation in a concerted study.

Recently, using a stable isotope labeling by amino acids in cell culture (SILAC) based proteomics Larance et al. comprehensively identified proteome-wide changes in response to starvation that included changes in proteins involved in chromatin organization, cell cycle, locomotion, life span and key metabolic pathways such as fatty acid degradation (Larance et al., 2015). In the present study we have used label-free quantitative proteomics in combination with RNA-sequencing (RNA-seq) to further disentangle starvation responses in a temporal manner with high resolution at the proteomic as well as at the transcriptomic level. We find only a moderate, and in some cases an inverse, correlation between mRNA and protein levels, arguing that not only transcriptional but also substantial posttranslational mechanisms contribute to the starvation

response. Furthermore, we show that the transcription factor HLH-30 serves key functions in the response and adaptation to starvation for example by modulating intestinal lipid transport and the expression of lipoproteins. Compared with other datasets, the present study provides comprehensive information about absolute gene and mRNA abundances and thus constitutes an important resource that allows detailed quantitative analyses of starvation responses. In support of open access data sharing all of the raw MS data from this study have been deposited to the ProteomeXchange Consortium 5 (http://proteomecentral.proteomexchange.org) via the MassIVE partner repository. Moreover, the processed proteomic data can be accessed in a searchable, online database (https://www.peptracker.com/epd/).

RESULTS

A systematic label-free quantitative proteome analysis of *C. elegans* charts the temporal starvation response

To further identify the molecular mechanisms governing the response and adaptation to starvation we aimed at uncovering proteomic changes in response to acute starvation using *C. elegans* as model organism. We therefore analyzed the temporal response to starvation across a 1 hour to 16 hours food deprivation time course (Figure 1A). We analyzed more time points within the first 6 hours to delineate early starvation responses with high resolution but also analyzed the response at 16 hours of food deprivation, where starvation induced changes in protein abundance reach their maximum (Larance et al., 2015). To complement the proteomic analyses we also examined the molecular responses to starvation at a transcriptional level by RNA-seq. Furthermore, in addition to studying wild type animals, we also analyzed the temporal starvation response in animals lacking the helix-loop-helix transcription factor HLH-30, which was previously shown to play important roles in adaptation to starvation (O'Rourke and Ruvkun, 2013). Thus, we starved worms from the mid-L4 stage by transferring a population of developmentally synchronous worms to unseeded NGM plates and sampled animals for proteomics and transcriptomic analyses after 1,

2, 3, 4, 6, and 16 hours. Since acute starvation of mid-L4 animals results in L4 arrest (Angelo and Van Gilst, 2009) we used fed mid-L4 animals as a point of reference. We harvested animals in biological triplicates for each condition and divided them into two identical pools, which were subjected to label-free MS-based proteomics and mRNA-seq based transcriptomics.

Using a two dimensional liquid chromatography-mass spectrometry (2D-LC-MS) label-free quantitative proteomic approach we identified 32,844 distinct peptides with a false discovery rate (FDR) of 1 %, distributed among ~4,580 proteins depending on the time point, and of these, at least two peptides were detected for 3,786 proteins. Across a total of 42 samples, we obtained a data completeness of 99.4%. The dynamic range of absolute protein abundance across all proteins was ~8 orders of magnitude, from approximately 10^{-5} fmol/ug to 1,400 fmol/ug (Figure S1). Among the most abundant proteins, we observed elongation factors including elongation factor 1-alpha (EFT-3) and elongation factor 2 (EEF-2) as well as several ribosomal subunits including 60S acidic ribosomal protein P1 (RLA-1), P2 (RPA-2), and 40S ribosomal protein SA (RPS-0) (data not shown).

We evaluated biological reproducibility by comparing the three biological replicates individually by Pearson correlation analyses for all time points (Figures S2A and S2B). We found high reproducibility between samples harvested at the same time point (R>0.94, Pearson), and that the correlation was higher at early time points of starvation compared with the latest time point (16 hours). As shown in the Venn diagrams more than 99% of proteins were identified in all three replicates of each condition (Figure 1B). Protein density and volcano plots show that the proteome changes substantially after 4, 6, and 16 hours of starvation in both wild type and *hlh-30* animals (Figure 1C and Figure 1D). To corroborate these data we assessed the level of proteins previously reported regulated by starvation (Larance et al., 2015; O'Rourke and Ruvkun, 2013; Settembre et al., 2013). Consistently, we observed that proteins involved in autophagy including ATG-18, ATG-4.1, EPG-6, and LGG-1 were up-regulated in wild type animals in response to 16 hours of starvation, whereas a number of key anabolic genes involved in fatty acid biosynthesis, including

POD-2 and FASN-1, encoding acetyl-CoA carboxylase and fatty acid synthase, respectively, as well as fatty acid desaturases (FAT-1 and FAT-4) were significantly down-regulated (Figure S3).

Acute starvation induces global metabolic changes in *C. elegans*

To systematically assess starvation-induced changes and identify groups of proteins that show a similar abundance profile during starvation, we subjected the proteomic datasets to hierarchical clustering based on Ward' minimum variance method (Murtagh and Legendre, 2014), visualized in a heat map (Figure 2A). To remove background noise, we filtered the data for proteins that had a q-value below 0.05 relative to fed wild type (t = 0 hours), in at least one time point, which reduced the data set to 1,780 proteins. To minimize redundancy in clustering due to large differences in abundances, the $\log_2$ protein ratios with respect to time point zero (fed) were scaled. This identified 4 distinct abundance profiles (Figure 2). Cluster I comprises proteins, that increase over time, reaching a high level after 16 hours; cluster II comprises proteins, that gradually increase in abundance over time; cluster III comprises proteins that continuously decrease in abundance that declines substantially after 16 hours; finally cluster IV comprises proteins that gradually decrease in abundance over time (Figure 2A).

Using DAVID (version 6.8 Beta) (Huang da et al., 2009a, b) we identified the enriched KEGG (Kyoto Encyclopedia of Genes and Genomes) pathways within each cluster (Figure 2B). Among the KEGG pathways enriched in cluster I we identified several catabolic pathways, which, expectedly, were up-regulated during starvation including "peroxisome", "lysosome", and "fatty acid degradation". Clusters I and II also contain several autophagy related proteins including LGG-1, DAF-15, EPG-6, ATG-18 and SQST-2 (Figure 2A). Interestingly, we found the two negative regulators of autophagy, i.e. TOR ortholog LET-363 and the DAP-1 ortholog, T28F4.5, were both contained in cluster II, indicating that degradation processes must be kept in check by inhibition during prolonged starvation. We also found that pathways including "spliceosome", "RNA polymerase", and "RNA transport" were enriched among the proteins contained in both cluster I

and II. Collectively, these data indicates that catabolic energy-producing pathways are up-regulated, and that extensive rewiring of translation and RNA processing occurs in response to starvation. We found among the enriched KEGG pathways in cluster III "protein processing in endoplasmic reticulum", "protein export", "ribosome", "biosynthesis of amino acids" and in general metabolism of amino acids. Interestingly, a recent study identified several ribosomal subunits down-regulated at the protein level in DR animals (Depuydt et al., 2013). We observe the tRNA synthetases CARS-1, WARS-1, RARS-1, and FARS-1 in clusters III and IV (Figure 2A). In cluster III we found "pentose phosphate pathway" enriched, which provides building blocks for RNA and DNA synthesis as well as the reducing redox equivalent NADPH for biosynthetic purposes including *de novo* fatty acid synthesis. Accordingly, although not enriched in specific KEGG pathways, we found several proteins involved in fatty acid synthesis, desaturation and elongation and phospholipid synthesis in cluster III and IV, including POD-2, FASN-1, SAMS-1, ELO-1, ELO-5, FAT-4, and FAT-6.

By subjecting the most up- and down-regulated (>2 fold, q-value < 0.05) proteins at each time point to Gene Ontology (GO) term enrichment analysis by DAVID (version 6.8 Beta) we also found that specific GO terms including "fatty acid metabolism" and "regulation of autophagy", were consistently enriched among the up-regulated proteins (Figure S4A), while GO terms related to numerous biosynthetic pathways were enriched among the down-regulated proteins beginning already at 2 hours of starvation (Figure S4B). Interestingly, the GO terms "negative regulation of proteolysis" was also enriched among the up-regulated proteins. This GO term comprise several serpins including SRP-2, -6, and -7, which are predicted to function as suicide substrates that inhibit the proteolytic activity of serine proteases (Pak et al., 2004). This suggests that proteolytic processes are kept in control during starvation by increasing the abundance of competitive substrates. In contrast with the KEGG pathway analysis, GO term enrichment analyses also revealed that GO terms including "metabolic process", "immune system process" and "innate immune response", were enriched among the down-regulated proteins (Figures S4B). These

proteins include UDP-glucuronosyl transferases (UGT-16, -21, -25, -41, 45, -57, -61), cytochrome P450 protein family members (CYP-25A2, -35A2, -35A3, -35C1), transcriptional regulators, and antimicrobial peptides, which all are involved in host immune responses (Simonsen et al., 2012). Collectively, these observations suggest a reduced investment in energy consuming pathways that do not contribute directly to survival of starvation including immune response pathways. As expected, we found that catabolic processes including fatty acid degradation, proteolysis and autophagy are induced, albeit not until several hours after initiation of starvation, while anabolic pathways and translation are dampened upon starvation.

Starvation induces profound transcriptional changes

To complement the proteomics analyses we employed RNA-seq to examine the transcriptional response to starvation. Analyzing the same populations of worms, we identified a total of 40,942 annotated RNAs encoding 20,381 proteins. The fraction of mRNA encoding protein detected from each of the 6 chromosomes closely matched previously published data (Consortium, 1998) (Figure S5). The numbers of protein-encoding RNAs identified in the triplicate samples at each time point are high (Figures 3A). Volcano plots indicated that the majority of the mRNAs increased in response to starvation in both wild type and in *hlh-30* animals (Figures 3B). Consistently, we found markedly more up-regulated than down-regulated RNAs, while in contrast the number of proteins that are up- and down-regulated is similar (Figure S6).

The 20,381 protein encoding mRNAs were matched to 18,966 corresponding UniProt accession numbers using the DAVID Gene ID Conversion Tool (Huang da et al., 2009a, b) (Table S1). We found a total overlap of 3,083 IDs, which were identified by both RNA-seq and proteomics. Furthermore, in accordance with previous reports (Azimifar et al., 2014; Grun et al., 2014; Ly et al., 2014; Maier et al., 2011; Vogel and Marcotte, 2012), we found that the Pearson correlation coefficient between mRNA and the corresponding protein (Figure 3C) was positive but moderate, ranging from 0.546 to 0.609 at different time points. Interestingly, we observed that the

abundances of some proteins correlated inversely with the abundance of their corresponding mRNA e.g. fatty acid desaturases (Figure S7). Thus, since it is level and activity of each protein in a proteome that define cellular and organismal phenotypes, these observations emphasizes the importance of not solely relying on mRNA data to infer protein levels, but to actually determine protein levels to understand phenotypic changes.

Hierarchical clustering of the 3,083 IDs shared between the mRNA and protein datasets using correlation distances for distance metric and Ward's minimum variance method, revealed 4 separate abundance profiles (Figure 4A). This further illustrates the inverse correlation between the abundances of some proteins and their corresponding mRNAs (Figure 4A). This analysis combined information for all proteins matched with their corresponding mRNAs as $\log_2$ ratios, with respect to fed animals (t = 0). Cluster I represents a group of proteins showing little or no decrease in abundance, whereas the abundance of their corresponding mRNAs shows a pronounced reduction during the course of starvation. Cluster II represents proteins that increase in abundance during starvation, with little or no increase in the corresponding mRNAs. Cluster III represents proteins that show a general and consistent decrease in abundance throughout starvation, whereas the corresponding mRNAs show a slight, but consistent increase, with a sub-cluster that peaks after 2 hours. Finally, cluster IV contains proteins showing minimal change in abundance, whereas the corresponding mRNAs show a consistent increase throughout starvation.

From these data it is obvious that the abundance levels of numerous proteins that we have identified are regulated differently than the corresponding mRNAs. Specifically, a subset of protein groups and corresponding mRNAs were identified that respond differently to starvation, rather than general trend throughout the entire proteome and transcriptome. This prompted us to examine the 4 clusters further. Thus we subjected the proteins in each cluster to KEGG pathway enrichment analyses, using DAVID as described above (Figure 4B). Among the enriched KEGG pathways in cluster I we identified several catabolic pathways including "Proteasome", "Oxidative phosphorylation" and "Citrate cycle (TCA cycle)", but also anabolic pathways including "Fatty acid

elongation" and "Ribosome". This suggests that the abundance of proteins involved in these pathways is less affected by starvation, while the abundance of the corresponding RNA is down-regulated. Cluster II comprises pathways also contained in cluster I of the proteome heat map (Figure 2A), including the catabolic pathways "Lysosome" and "Fatty acid degradation".

Cluster III, like clusters I and II of the proteome heat map (Figure 2A), contains several mRNA processing related pathways such as "Spliceosome" and "mRNA surveillance pathway". However, in contrast with the clusters discussed above (I and II, Figure 2A), the abundance of proteins in cluster III decrease with time of starvation, whereas the corresponding mRNA levels are slightly increasing during starvation and stabilizing after 16 hours. Altogether, these observations suggest a complex pattern, involving both upregulation and downregulation of abundance levels for different proteins involved in RNA processing with the latter group of proteins also showing increased mRNA levels. Interestingly, the KEGG pathway "Ribosome biogenesis in eukaryotes" is enriched in both clusters III and IV, which indicates that the organism responds to starvation by reducing translation at the protein level while continuously transcribing the corresponding mRNA. A possible reason for this could be to potentially allow a fast response to growth when nutrient availability increases again post starvation. These observations are in line with previous studies in dietary restricted animals (Depuydt et al., 2013). Cluster IV contains KEGG pathways related to both catabolic (including "Fatty acid degradation" and "Peroxisome") and anabolic (including "Biosynthesis of amino acids" and "One carbon pool by folate) functions, again implying that the organism is preparing for the potential return of nutrients by transcription of genes involved in these pathways without the subsequent translation resulting in a steady level of the corresponding proteins. Strikingly, cluster IV also comprises the fatty acid desaturases *fat-1, 2, 4* and *-6* whose mRNA increase in response to starvation as previously reported (Settembre et al., 2013), while we observe that the abundance of the corresponding proteins decrease (Figure S7). Interestingly, the pathways "Endocytosis" and "SNARE interactions in vesicular transport" are also contained in

cluster IV, suggesting that also the potential uptake of nutrients by endocytosis is up-regulated at the transcriptional level while showing little or no changed at the protein abundance level.

Despite the moderate correlation observed between protein and mRNA abundance, analysis of transcriptional responses can still illuminate valuable phenotypic information showing how an organism responds to starvation, and also serves as a valuable indicator for future studies. Hence, we subjected the significantly up- or down-regulated transcripts (significance in this case being defined as q-value < 0.05, > 2-fold change) found at each time point relative to fed wild type levels (t = 0) to GO term enrichment analysis using DAVID (version 6.8 Beta) as for the proteomics data above. As expected, the number of enriched GO terms increases over time; however, while GO terms among the up-regulated RNAs are enriched already after 1 hour, we do not observe enriched GO terms among the down-regulated RNAs until 3 hours post starvation onset (Figure S8A and Figure S8B).

Interestingly, GO terms describing defense responses involving responses to either a bacterial or biotic stimulus, were highly enriched among the up-regulated RNAs, while GO terms relating to innate immune responses were among the down-regulated RNAs (Figure S8A and Figure S8B). Although less prominent, we also identify the GO term “cellular response to stimulus” to be significantly enriched among the up-regulated genes, which interestingly, included 15 members of nuclear hormone receptor (NHR) family. Such massive induction of NHRs during food deprivation suggests that they play an important role in the transcriptional response to starvation. Consistent with this idea, it has recently been shown that ~10% of the 293 NHR encoding genes are up-regulated upon starvation and down-regulated upon subsequent re-feeding at the transcriptional level (Hyun et al., 2016). Accordingly, despite that we did not detect *nhr-45* and *nhr-49* at the mRNA level, we identified both of them to be up-regulated at the protein level. Both NHR-45 and NHR-49 have previously been found to be involved in starvation responses (Arda et al., 2010; Van Gilst et al., 2005). In support of this notion, GO terms “lipid metabolic process” and “fatty acid metabolic process”, which include putative NHR-49 target genes, e.g. *acs-2*, *acdh-6*, the FAXDC2

ortholog *f49e12.10*, and 3-hydroxyacyl-CoAdehydrogenase *f21c10.10* were also enriched among the significantly up-regulated mRNAs after 16 hours of starvation.

Functional loss of HLH-30 induces global proteomic changes

The transcription factor HLH-30 and its mammalian ortholog TFEB have previously been shown to serve crucial functions during starvation, dietary restriction and autophagy in both *C. elegans* and in mammals (Lapierre et al., 2013; Magini et al., 2013; O'Rourke and Ruvkun, 2013; Pena-Llopis et al., 2011; Roczniak-Ferguson et al., 2012; Settembre et al., 2013; Wang et al., 2015). However, most of these analyses have been performed at a genomic level and not at a proteomic level *per se*. Thus, we examined the role of the *C. elegans* orthologue of the transcription factor HLH-30 during starvation. Based on our proteomics data, we sought to identify proteins and pathways responding to starvation in the wild type population that showed an altered or lacking response in mutant animals. Since we were interested in the temporal response to starvation, we first chose to focus on effects persisting over time rather than considering changes in abundance only detected at isolated time points. To identify differences in how wild type animals and *hlh-30* animals respond to starvation, we calculated a score based on the change in abundance over time and the difference in protein abundance between wild type and the *hlh-30* mutant:

$$Score = (1 - |A|) \times B$$

where *A* is the Pearson correlation between the temporal response curves for a given protein over time between wild type and mutant, and *B* is the integrated numerical difference between the same curves. Thus, for a certain protein, whose abundance does not correlate over time between strains, *A* will tend to 0. To focus on proteins that had either a reduced or increased response to starvation in *hlh-30* animals, we aimed at identifying proteins where A was close to 0. Since *B* describes the absolute area between the wild type and mutant over time, a high value of *B* suggests a large difference in abundance for a given protein between the two strains. To diminish the impact from a potential large difference in abundance between two specific proteins in the two populations, we

normalized protein levels of each time point and for both conditions with respect to protein levels in fed wild type animals at time point 0 and transformed them to $\log_2$ ratios. Thus, the $\log_2$ ratio is 0 at the first time point for the wild type, but may differ for *hlh-30* animals.

Based on the correlation and the absolute integrated area between the curves, we show four examples of known HLH-30 regulated genes, including the correlation and absolute integrated value (Figure S9A). To further corroborate this approach and to identify proteins regulated by starvation in an HLH-30-dependent and temporal manner, we therefore calculated and plotted the score of all identified proteins including known HLH-30 targets, e.g. ATG-18, LGG-1, CPR-1, VPS-18 and HLH-30 itself. Interestingly, these all had a score >1.03, which was above the 75th percentile of the score for all proteins (Figure S10A). However, we observed a fairly uniform distribution of the *A* component (Figure 5A), indicating that the correlation only slightly contributes to the total score. As we observed a large value for *B* for a number of proteins previously described as HLH-30 targets, we argue that it is the absolute abundance rather than temporal fluctuations at the protein level that is affected by the absence of HLH-30. Thus, by selecting proteins with a high *B* value, rather than a high total score (*B* value >1.85, 75th percentile, Figure S10B), we identified 1,109 proteins, which include targets whose expression has previously been shown to depend on HLH-30 (Figure 5 and Figure S9). By KEGG pathway enrichment analysis using DAVID (version 6.8 Beta), we functionally classified the 1,109 proteins to pathways that included “metabolic pathways” and cytochrome P450 pathways (Figure 5). Enriched GO terms were primarily associated to developmental and reproductive processes, possibly reflecting that loss of HLH-30 affects survival during starvation (O'Rourke and Ruvkun, 2013). We also noted that GO terms associated with defense mechanisms and innate immune response were enriched when a similar analysis was performed using RNA abundances instead of protein abundance (Figure 5D). Interestingly, comparing the GO terms which are enriched by using protein and RNA abundance, respectively, we noted that “lipid localization” was the only shared enriched GO term (Figure 5C

and Figure 5D). This GO-term included proteins such as, e.g. CCO-1, LPD-3, CCG-1, MDT-15, OBR-1 and VIT-1,-2,-3, and -4 (Table S1).

Vitellogenins are required for acute starvation survival

Vitellogenins are precursors of yolk proteins, synthesized in the intestine, secreted to the body cavity and taken up in the gonad were they accumulate in the oocytes (Blumenthal et al., 1984; Kimble and Sharrock, 1983). Vitellogenins are known to increase with age (Liang et al., 2014) and have previously been linked to aging in *C. elegans* (Murphy et al., 2003; Seah et al., 2016), as well as in other organisms (Tetlak et al., 2015). Vitellogenins play crucial roles in lipid transport and control trafficking of lipids, either for energy production in the starving hermaphrodite or for reproduction in the oocytes. Consistent with recent findings (Heestand et al., 2013; Seah et al., 2016), we also find that vitellogenins are down-regulated after a few hours of starvation (Figure S11).

Since we find that the vitellogenins show an inverse response to starvation in *hlh-30* as opposed to wild type animals and that HLH-30 is required for survival under starvation conditions (O'Rourke and Ruvkun, 2013), we asked if the vitellogenins are required for survival in response to acute starvation. As previously reported (O'Rourke and Ruvkun, 2013), we also found that the *hlh-30* mutant dies prematurely under such conditions (Figure 6). Surprisingly, knock down of *vit-1* and *vit-5* rescued the short-lived phenotype of *hlh-30* animals in response to acute starvation, but had no effect on survival of wild type animals during starvation conditions (Figure 5). Interestingly, among the HLH-30 dependent proteins, we also identified SSQ-4 and UNC-41. Analogous to the vitellogenins, we found both these proteins induce a similar phenotype when knocked down in *hlh-30* animals (Figure 6). Knowing that the vitellogenins play important functions in lipid transport and storage prompted us to assess the distribution of intestinal lipid droplets in both wild-type and in *hlh-30* animals. Coherent Anti-stokes Raman Scattering (CARS) microscopy revealed that the size of intestinal lipid droplets in the wild type increased over time of starvation compared to fed

animals, while the number of droplets decreased during starvation (Figure 7), as previously shown in dietary restricted animals (Palgunow et al., 2012). When examining lipid droplets in *hlh-30* animals during starvation we observed an opposite response (Figure 7). Interestingly, knock down of *vit-1* in *hlh-30* animals completely restored the size and number of lipid droplets, while having little or no effect in wild type animals. Altogether, our data indicate that nutrient levels balance the number and size of intestinal lipid droplets, which can be modulated by HLH-30 and vitellogenins.

In conclusion, the present study demonstrates how systems-wide analyses can provide functional insights into novel regulatory mechanisms controlling fundamental processes that links metabolism and survival in metazoans. It also emphasizes the importance of examining fundamental regulatory mechanisms by addressing protein abundances and not only formulate new models based on RNA abundances. We anticipate that the present in-depth resource will inspire and enable additional studies in starvation responses in metazoans.

DISCUSSION

In the present study we have applied 2D-LC-MS/MS label-free quantitative proteomics and RNA-seq to globally monitor temporal changes in protein- and mRNA levels in response to starvation in both wild type *C. elegans* and in animals lacking functional HLH-30, a homologue of the mammalian transcription factor TFEB. In each of three biological replicates (Figure 1A), we identified >4,500 proteins, with at least two peptides detected in ~3,800 proteins per time point and with >99% data coverage across all time points. Moreover, >99% of the identified proteins were detected and quantified in all three replicates at each time point. A recent study also examined the temporal response to starvation in *C. elegans* using SILAC-based proteomics and reported identification of ~5,500 proteins in all samples from both fed and starved animals, across all time points (Larance et al., 2015). Although we identify fewer proteins in the present study, our analyses provide measurement of absolute levels of each protein. Thus, we show that the absolute protein

abundance in all samples spans approximately 8 orders of magnitude ranging from approximately 10^{-5} fmol/ug to 1,400 fmol/ug.

Our present analyses provide a valuable, in-depth resource that identifies multiple physiological responses to starvation, including lipid- and amino acid metabolism, stress responses, and autophagy. Dynamic changes in protein abundances allow an organism to adapt its metabolism to nutritional and environmental changes, e.g. by down-regulating anabolic pathways and upregulating catabolic pathways. Consistent with previous findings and the notion that anabolic processes are suppressed in response to nutrient deprivation, we detect numerous proteins involved in *de novo* biosynthesis and desaturation of fatty acids that are down-regulated in response to starvation. This includes POD-2/ACC, the enzyme catalyzing the rate-limiting step in *de novo* fatty acid synthesis, fatty acid synthase FASN-1 and fatty acid desaturases like FAT-1, FAT-2, FAT-4, and FAT-6 (Larance et al., 2015; Pang et al., 2014). Moreover, the two long-chain acyl-CoA synthetases, ACS-1 and ACS-2, are involved in lipid biosynthetic and degradative pathways, respectively (Zhang et al., 2011; Zhang et al., 2013). Interestingly, we find that their abundance is down- and up-regulated, respectively, suggesting that metabolically active fatty acids are re-directed towards degradation.

In agreement with previous findings (Larance et al., 2015), we also find that a number of enzymes that metabolizes either short-, or medium chain, fatty acids are down-regulated during starvation, while the abundance of proteins involved in mitochondrial import of long-chain acyl-CoA esters (e.g. CPT-1), remains unchanged during starvation (Figure 4). Thus, we conclude that down-regulation of POD-2/ACC and consequently the synthesis of malonyl-CoA, a potent inhibitor of CPT-1, likely determines the rate of fatty acid oxidation in fasting animals. However, posttranslational protein modifications are likely also to contribute to the control of fatty acid degradation. Narbonne and Roy have previously shown that AMPK can phosphorylate and inhibit the triacylglycerol lipase ATGL-1, which rations lipid stores during dauer (Narbonne and Roy, 2009). Such regulatory mechanisms may very likely also control mobilization of fat stores during

starvation in older animals because starvation of adult animals causes an increase in the AMP:ATP ratio, which activates AMPK (Apfeld et al., 2004).

Only a few studies have combined quantitative proteomics with RNA-seq in *C. elegans* (Grun et al., 2014; Ma et al., 2014; Yang et al., 2015). Consistent with these previous observations, we also find that transcript levels show only a moderate correlation with protein levels for the bulk proteome and transcriptome (Figure 3C). This indicates that protein abundances are not only determined by transcript levels and transcriptional activity, but also via regulatory mechanisms affecting rates of translation, protein stability, and turnover. Most strikingly, we observe an increase in the levels of mRNAs encoding the fatty acid desaturases *fat-1, 2, 4* and *-6* in response to starvation, as previously reported (Settembre et al., 2013), while we observe a decrease in the abundance of the corresponding proteins (Figure S7). To this end, the starvation-induced increase in *fat-6* mRNA depends on the presence of HLH-30, while FAT-6 protein abundance is independent on the presence of HLH-30. Given the fact that proteins are likely to regulate cellular processes and metabolic fluxes, our study therefore emphasizes the importance of directly measuring and evaluating protein levels, rather than relying upon measurements of mRNA levels as a surrogate for proteins, because relying solely on RNA abundance can lead to misinterpretations of regulatory mechanisms and of phenotypic outputs.

The mammalian transcription factor EB (TFEB) and its homologue in *C. elegans* HLH-30 have both been shown to regulate autophagy, lysosomal functions and lipid metabolism (Lapierre et al., 2013; O'Rourke and Ruvkun, 2013; Settembre et al., 2013; Settembre et al., 2011). Whiles these studies primarily were based on genetic analyses, HLH-30 functions had not previously been examined by proteomics. Thus, to identify which proteins respond differently to starvation in the wild type animals and the *hlh-30* mutants, we calculated a simple score based on protein abundances and changes in protein abundance over time during starvation. This analysis showed that it is primarily the absolute protein abundance rather than the temporal change that best identifies proteins whose abundance depends on HLH-30.

Comparing starvation responses in wild type and *hlh-30* mutants, we found several significantly enriched GO terms among the highest scoring proteins (Figure 4). This included "Lipid localization", a GO term encompassing several of the vitellogenins. Vitellogenesis describes the process where maternal yolk production provides the major nutrient source for the developing embryo. Vitellogenin genes are expressed in adult females within tissues specialized for yolk production, such as the insect fat body in fruit flies and in the intestine of *C. elegans*. Yolk is transported across the body cavity to the gonad, where it supplies developing oocytes with nutrients, including fat, until reproduction ceases. After reproduction, localization is no longer restricted to the intestine and oocytes, but instead extends throughout the organism, including the body cavity resulting in ectopic yolk deposition and hence loss of tissue function (Van Rompay et al., 2015; Zimmerman et al., 2015). Consistently, knock down of vitellogenins increases *C. elegans* lifespan (Seah et al., 2016), and levels of yolk protein are reduced in post-reproductive adults of long-lived *daf-2* animals (DePina et al., 2011). Thus, to further uncover the function of the *vit*-genes during starvation we examined the ability to survive in response to acute starvation after RNAi knock down of *vit-1* and *vit-5* in both wild type and in *hlh-30* animals. Curiously, we found that knock-down of either *vit-1*, or *vit-5*, did not affect survival of wild type animals, while knock down completely rescued the premature death of *hlh*-30 animals under starvation conditions (Figure 6, Table 1). Since we found that *vit-1* knock down did not affect either the number, or size, of intestinal lipid droplets in wild type animals, but normalized their size and number in *hlh-30* animals (Figure 7), we speculate that loss of vitellogenins prevents ectopic deposition of lipids in *hlh-30* animals and consequently improves survival. In *eat-2* animals, which are inherently dietary restricted, it has been reported that the expression of >2,900 genes are altered compared with wild type animals, which includes genes involved in phosphorus metabolism, unsaturated fatty acid metabolism, eicosanoid and ceramide metabolism, lipid modification and transport, amino acid, amine and chitin metabolism and neuropeptide signaling (Heestand et al., 2013). Loss of *nhr-62* reversed the regulation of ~ 600 of these genes, including *vit-1* through *vit-6*, arguing that these genes are candidate targets for NHR-62 and play key roles in response to dietary restriction.

Hence, our present analyses suggest that HLH-30 also regulates the expression of the *vit*-genes and further argue that vitellogenins play fundamental roles under limiting nutrient levels.

Visvikis et al. recently identified HLH-30 and its mammalian homologue TFEB as a key transcriptional regulator of the early innate immune response involving antimicrobials and cytoprotective responses (Visvikis et al., 2014). Interestingly, lipoprotein metabolism and the innate immune systems are increasingly being recognized as being functionally linked. Despite it is yet to be identified in *C. elegans*, lipoproteins are via their ability of binding lipopolysaccharide (LPS) capable of protecting against LPS-induced toxicity, and to modulate the overall host response to this bacterial toxin (Barcia and Harris, 2005). We can therefore not exclude that the normalized distribution of intestinal lipid droplets in *hlh-30* animals after *vit-1* knock down contributes to host defense responses and thus improved survival under stress-full conditions.

Collectively, this study provides the first comprehensive analysis of temporal starvation responses that combines both proteomic and transcriptomic analyses. To maximize the value of these data for the research community we have incorporated all of the processed proteomics and RNA data showing responses to starvation in both wild type and *hlh-30* animals into an open access, searchable online database (www.peptracker.com/epd). We foresee that the datasets not only will serve as a key resource for the scientific community for further understanding how *C. elegans* responds and adapts to starvation, but also accentuate the relevance of a combined analysis of transcript and protein levels in understanding of complex phenotypic responses. We envision that the genetic tractability of *C. elegans*, RNA interference, and mutant strain collections can serve as an excellent framework to further delineate how specific genes regulate starvation responses.

EXPERIMENTAL PROCEDURES

C. elegans strains and maintenance

The wild type N2 Bristol and the *hlh-30* mutant (tm1978, a kind gift from Dr. Malene Hansen, Sanford-Burnham Medical Research Institute) were used and handled using standard techniques (Brenner, 1974). Worms were at all times kept at 20 ^{0}C on NGM plates seeded with *E. coli* OP50. For starvation studies, worms were washed off seeded plates with M9 buffer and washed 2-3 times. Worms were transferred to empty NGM plates and starved for the indicated time.

Sample preparation for mass spectrometry

Worms were harvested in M9 buffer, pelleted by centrifugation, and all supernatant was removed. The pellet of worms was flash frozen in liquid nitrogen and stored at -80 °C. Worm pellets were fast-thawed in an 80 °C water bath and 50 µL pre-heated protein lysis, reduction and alkylation buffer was added to a final concentration of 1% sodium deoxycholate (SDC), 10mM tris(2-carboxyethyl)phosphoine (TCEP), 40mM chloroacetaldehyde (CAA)). Worms were lysed by cycles of tip sonication (Branson 2200), heating (80 °C) and vortexing. The protein concentration was measured by amino acid analysis (AAA) using a Biochrom 30 amino acid analyzer (Biochrom) as described (Hojrup, 2015). Proteins were digested with trypsin using the ISD:SDC(PT) protocol as described (Leon et al., 2013) with minor modifications. Briefly, 100 µg of protein per time point was digested with trypsin (1:50) at 37^{0}C for 10 hours and subsequently dimethyl sulfoxide (DMSO) was added (10% final concentration) followed by 400uL ethyl acetate and TFA (0.25% final concentration) for phase-transfer clean-up of the digests. After centrifugation for 10 minutes at 14,000 x *g*, the peptide containing lower phase was transferred to a new tube and stored at -80 °C until analysed.

LC-MS/MS

Protein digests (about 500 ng) were mixed with 50 fmol of the synthetic *E. coli* ClpB internal protein standard (Waters Corporation, Milford, MA, USA), to afterwards enable estimation of absolute protein abundances by label-free quantification. Peptide separation was performed with an Ultimate 3000 nano UPLC system (Thermo Fisher Scientific, San Jose, CA, USA) fitted with a 2

cm, 180 µm ID Symmetry C18 trap column (Waters) and a 25 cm, 75 µM ID, BEH C18 (1,7 µM particles) analytical column (Waters). Peptides were trapped for 2 min at 15 µl/min with 0.1% TFA and separated at 350 nl/min using a 60 min gradient of 4-35% acetonitrile with 0.1% formic acid. Eluting peptides were ionized at 1.7 kV using a TriVersa NanoMate (Advion Biosciences, Ithaca, NY, USA) as nanoelectrospray ion source coupled to an Orbitrap Fusion mass spectrometer (Thermo Fischer Scientific). Full MS scans (350 to 1500 *m*/*z*) were acquired at 120,000 resolution (at 200 *m*/*z*) from 350 to 1500 *m*/*z* with wide window quadrupole isolation turned on. Full scan target was 5×10^5 with a maximum fill time of 100 ms and all data was acquired in profile mode using positive polarity. For tandem MS the instrument was run in top speed mode with maximum 5 s cycles selecting precursors above 1×10^5 intensity with charge state 2–6. Targets were isolated at 0.7 Th using the quadrupole followed by HCD fragmentation with normalized collision energy of 28 and rapid scan MS analysis in the ion trap. The MS2 ion AGC target was 1×10^4 with a maximum fill time of 30 ms and using the all-parallelizable-time (APT) option. Attempting to increase the overall experimental sensitivity and depth, a method variant was used alternating between each sample, using a maximum fill time of 45 ms combined with the only-single-charge-state-per-precursor option. For both methods the dynamic exclusion time was set to 25 s with a 10 ppm tolerance.

Database searching and quantification

Proteome Discoverer v1.4.0.288 (Thermo Fischer Scientific) was used to process the raw data files and perform database searches on an in-house Mascot server, version 2.3 (Matrix Science, London, UK). Fragmentation spectra were searched against a fasta formatted database containing all canonical UniProtKB entries for *Caenorhabditis elegans*, version 0214 (February 2014), with common contaminants and protein quantitation standards (26700 entries in total). Trypsin was selected as enzyme, allowing up to 2 missed cleavages with carbamidomethylation of cysteines as fixed modifications, and methionine oxidation and protein N-terminal acetylation as variable modifications. Search tolerances were set to 10 ppm for peptide precursors and 0.35 Da for

fragment ion masses. Peptide identifications were validated and filtered at 1% false discovery rate on peptide level using the percolator tool (Brosch et al., 2009) or (Spivak et al., 2009). Progenesis QI for proteomics v2.0 (Waters and/or Nonlinear Dynamics, UK) was used for label-free absolute protein quantification. All raw files were first imported and aligned followed by import and matching of the Proteome Discoverer search results. Absolute quantification was achieved by using the built in feature based on the Hi3 method (Silva et al., 2006) and the known amount of spiked-in protein standard.

For the calculation of fmol/µg the M_W of each protein was found using the online tool http://web.expasy.org/compute_pi/ (Bjellqvist et al., 1994; Bjellqvist et al., 1993; Wilkins et al., 1999). The total amount of protein (µg) in each probe was summed and the fmol OC values were divided by the median of the total amount of protein across all samples. The R language (RStudio version 0.98.1103) was used for further data analysis and figure preparation. *q*-values of the limma Rank product were calculated using the R script described in (Schwammle et al., 2013). To assign a biological function to significantly regulated proteins, the lists were subjected to the Gene Functional Classification tool of DAVID (version 6.8 Beta) (Huang da et al., 2009a, b).

RNA extraction and RNA-seq

Worm pellet was fast-thawed in 65^{0}C water bath. Worms were lysed by incubation in 1mL Isol-RNA Lysis Reagent (Ref #2302700 5 PRIME) and vortxed on/off for 20 min. 100 uL bromochorophenol was added, samples vigorously vortexed and incubated for 15 min at room temperature to extract the RNA. The two phases were separated by centrifugation for 15 min at 12,000xg at 4 °C. The upper phase containing the RNA was transferred to new tubes and 600uL isopropanol was added and samples were incubated for 10 min at room temperature to precipitate the RNA. The RNA was pelleted by centrifugation for 8 min at 12,000xg at 4^{0}C and the pellet washed several times in 70% ethanol. RNA was further cleaned using Qiagen RNeasy Protect Mini kit (Qiagen). For mRNA-seq 1µg total RNA was incubated with poly-dT beads to isolate

polyadenylated RNA, subjected to fragmentation and cDNA synthesis followed by library preparation (TruSeq RNA Sample Prep kit v2) performed according to the manufacturer's (Illumina) instructions. Sequencing was carried out on a HiSeq1500 platform (Illumina).

Data analysis of RNA-seq results

Sequencing reads were mapped to the ce6 genome with STAR (Dobin et al., 2013) and further analysed in HOMER (Heinz et al., 2010). Differential expression was determined using EdgeR (Love et al., 2014). The UCSC Genome Browser (Kent, 2002; Kent et al., 2002) was used for data visualization.

Survival-span assay

Worms were synchronized as described above. Eggs were transferred to plates containing RNAi bacteria for hatching. After hatching L1 larvae was kept on RNAi bacteria until L4 stage (54 h) and then transferred to empty NGM plates containing kanamycin to induce starvation condition. 12 worms were placed on each plate and scored every day. A worm was scored dead when it was unresponsive to gentle prodding with a platinum pick.

CARS microscopy

Worms were bleached as described above and the egg pellet was transferred to NGM plates seeded with either RNAi control (L4440) or gene specific RNAi bacteria. When worms reached young adulthood (14 h post L4) they were washed of plates and washed twice with sterile water to remove bacteria. Worms were placed on empty NGM plates containing kanamycin. At 3, 6 and 8 hours of starvation, approx. 20 worms were mounted on 2 % agarose pads containing 10 µL 20 mM tetramizole (dissolved in M9) and sealed with a cover slide. Lipid droplets were monitored by CARS microscopy using a Leica TCS SP8 system with a CARS laser, picoEmerald (OPO, >600 mW at 780 nm/940 nm, pulse width 5–6 ps, 80 MHz; pump, >750 mW at 1,064 nm, pulse length 7

ps, 80 MHz) and the LAS AF/X software. The lasers were adapted to the symmetrical C-H stretch range by tuning the pump beam to 816.4 nm while keeping the Stokes beam constant at 1,064.6 nm. The output of both lasers was set to 1.3 W and the scan speed to 400 Hz. Only signals from the epi-CARS and epi-SHG (second harmonic generation) detectors were collected. Images were processed using ImageJ (NIH), and the number and size of intestinal lipid droplets were determined using the Lipid droplet counter plugin.

ACKNOWLEDGEMENTS

This work was supported by The Danish Council for Independent Research, Natural Sciences (NJF: grant #310-95-23459). We gratefully acknowledge scientific discussions with Dr. Lea Mørch Harder and Dr. Dennis Pultz, (Institute of Biochemistry and Molecular Biology, University of Southern Denmark). We acknowledge Malene Hansen (Sanford-Burnham Medical Research Institute, CA, USA) for providing the tm1978 strain. We would like to gratefully thank Dr. Mark Larance (Centre for Gene Regulation and Expression, College of Life Science, University of Dundee) and Ole N. Jensen (Department of Biochemistry and Molecular Biology, University of Southern Denmark, Denmark) for practical assistance and scientific discussions. Furthermore, we would like to thank Anne With for practical laboratorial assistance and Alejandro Brenes Murillo for bioinformatics advice.

AUTHOR CONTRIBUTIONS

E.B.H., R.R.S., K.B.D. and N.J.F. designed experiments. E.B.H. and N.J.F. wrote the manuscript. E.B.H., R.R.S., R.N., and K.B.D. performed experiments and analyzed data. A.I.L., A.G., C.S.E., S.M. and N.J.F. oversaw the project.

REFERENCES

Angelo, G., and Van Gilst, M.R. (2009). Starvation protects germline stem cells and extends reproductive longevity in C. elegans. Science *326*, 954-958.

Apfeld, J., O'Connor, G., McDonagh, T., DiStefano, P.S., and Curtis, R. (2004). The AMP-activated protein kinase AAK-2 links energy levels and insulin-like signals to lifespan in C. elegans. Genes Dev *18*, 3004-3009.

Arda, H.E., Taubert, S., MacNeil, L.T., Conine, C.C., Tsuda, B., Van Gilst, M., Sequerra, R., Doucette-Stamm, L., Yamamoto, K.R., and Walhout, A.J. (2010). Functional modularity of nuclear hormone receptors in a Caenorhabditis elegans metabolic gene regulatory network. Mol Syst Biol *6*, 367.

Azimifar, S.B., Nagaraj, N., Cox, J., and Mann, M. (2014). Cell-type-resolved quantitative proteomics of murine liver. Cell metabolism *20*, 1076-1087.

Barcia, A.M., and Harris, H.W. (2005). Triglyceride-rich lipoproteins as agents of innate immunity. Clin Infect Dis *41 Suppl 7*, S498-503.

Bjellqvist, B., Basse, B., Olsen, E., and Celis, J.E. (1994). Reference points for comparisons of two-dimensional maps of proteins from different human cell types defined in a pH scale where isoelectric points correlate with polypeptide compositions. Electrophoresis *15*, 529-539.

Bjellqvist, B., Pasquali, C., Ravier, F., Sanchez, J.C., and Hochstrasser, D. (1993). A nonlinear wide-range immobilized pH gradient for two-dimensional electrophoresis and its definition in a relevant pH scale. Electrophoresis *14*, 1357-1365.

Blumenthal, T., Squire, M., Kirtland, S., Cane, J., Donegan, M., Spieth, J., and Sharrock, W. (1984). Cloning of a yolk protein gene family from Caenorhabditis elegans. J Mol Biol *174*, 1-18.

Brenner, S. (1974). The genetics of Caenorhabditis elegans. Genetics *77*, 71-94.

Brosch, M., Yu, L., Hubbard, T., and Choudhary, J. (2009). Accurate and sensitive peptide identification with Mascot Percolator. J Proteome Res *8*, 3176-3181.

Consortium, *C.e.*S. (1998). Genome sequence of the nematode *C. elegans*: a platform for investigating biology. Science *282*, 2012-2018.

Cuervo, A.M. (2013). Preventing lysosomal fat indigestion. Nature cell biology *15*, 565-567.

DePina, A.S., Iser, W.B., Park, S.S., Maudsley, S., Wilson, M.A., and Wolkow, C.A. (2011). Regulation of Caenorhabditis elegans vitellogenesis by DAF-2/IIS through separable transcriptional and posttranscriptional mechanisms. BMC Physiol *11*, 11.

Depuydt, G., Xie, F., Petyuk, V.A., Shanmugam, N., Smolders, A., Dhondt, I., Brewer, H.M., Camp, D.G., 2nd, Smith, R.D., and Braeckman, B.P. (2013). Reduced insulin/insulin-like growth factor-1 signaling and dietary restriction inhibit translation but preserve muscle mass in Caenorhabditis elegans. Mol Cell Proteomics *12*, 3624-3639.

Dobin, A., Davis, C.A., Schlesinger, F., Drenkow, J., Zaleski, C., Jha, S., Batut, P., Chaisson, M., and Gingeras, T.R. (2013). STAR: ultrafast universal RNA-seq aligner. Bioinformatics *29*, 15-21.

Dong, M.Q., Venable, J.D., Au, N., Xu, T., Park, S.K., Cociorva, D., Johnson, J.R., Dillin, A., and Yates, J.R., 3rd (2007). Quantitative mass spectrometry identifies insulin signaling targets in C. elegans. Science *317*, 660-663.

Elle, I.C., Rodkaer, S.V., Fredens, J., and Faergeman, N.J. (2012). A method for measuring fatty acid oxidation in C. elegans. Worm *1*, 26-30.

Fredens, J., Engholm-Keller, K., Giessing, A., Pultz, D., Larsen, M.R., Hojrup, P., Moller-Jensen, J., and Faergeman, N.J. (2011). Quantitative proteomics by amino acid labeling in C. elegans. Nat Methods *8*, 845-847.

Grun, D., Kirchner, M., Thierfelder, N., Stoeckius, M., Selbach, M., and Rajewsky, N. (2014). Conservation of mRNA and protein expression during development of C. elegans. Cell Rep *6*, 565-577.

Hansen, M., Taubert, S., Crawford, D., Libina, N., Lee, S.J., and Kenyon, C. (2007). Lifespan extension by conditions that inhibit translation in Caenorhabditis elegans. Aging Cell *6*, 95-110.
Heestand, B.N., Shen, Y., Liu, W., Magner, D.B., Storm, N., Meharg, C., Habermann, B., and Antebi, A. (2013). Dietary restriction induced longevity is mediated by nuclear receptor NHR-62 in Caenorhabditis elegans. PLoS Genet *9*, e1003651.
Heinz, S., Benner, C., Spann, N., Bertolino, E., Lin, Y.C., Laslo, P., Cheng, J.X., Murre, C., Singh, H., and Glass, C.K. (2010). Simple combinations of lineage-determining transcription factors prime cis-regulatory elements required for macrophage and B cell identities. Molecular cell *38*, 576-589.
Hojrup, P. (2015). Analysis of Peptides and Conjugates by Amino Acid Analysis. Methods Mol Biol *1348*, 65-76.
Huang da, W., Sherman, B.T., and Lempicki, R.A. (2009a). Bioinformatics enrichment tools: paths toward the comprehensive functional analysis of large gene lists. Nucleic acids research *37*, 1-13.
Huang da, W., Sherman, B.T., and Lempicki, R.A. (2009b). Systematic and integrative analysis of large gene lists using DAVID bioinformatics resources. Nat Protoc *4*, 44-57.
Hyun, M., Davis, K., Lee, I., Kim, J., Dumur, C., and You, Y.J. (2016). Fat Metabolism Regulates Satiety Behavior in C. elegans. Sci Rep *6*, 24841.
Kang, C., You, Y.J., and Avery, L. (2007). Dual roles of autophagy in the survival of Caenorhabditis elegans during starvation. Genes & development *21*, 2161-2171.
Kent, W.J. (2002). BLAT--the BLAST-like alignment tool. Genome Res *12*, 656-664.
Kent, W.J., Sugnet, C.W., Furey, T.S., Roskin, K.M., Pringle, T.H., Zahler, A.M., and Haussler, D. (2002). The human genome browser at UCSC. Genome Res *12*, 996-1006.
Kimble, J., and Sharrock, W.J. (1983). Tissue-specific synthesis of yolk proteins in Caenorhabditis elegans. Developmental biology *96*, 189-196.
Lapierre, L.R., De Magalhaes Filho, C.D., McQuary, P.R., Chu, C.C., Visvikis, O., Chang, J.T., Gelino, S., Ong, B., Davis, A.E., Irazoqui, J.E., et al. (2013). The TFEB orthologue HLH-30 regulates autophagy and modulates longevity in Caenorhabditis elegans. Nat Commun *4*, 2267.
Larance, M., Bailly, A.P., Pourkarimi, E., Hay, R.T., Buchanan, G., Coulthurst, S., Xirodimas, D.P., Gartner, A., and Lamond, A.I. (2011). Stable-isotope labeling with amino acids in nematodes. Nat Methods *8*, 849-851.
Larance, M., Pourkarimi, E., Wang, B., Brenes Murillo, A., Kent, R., Lamond, A.I., and Gartner, A. (2015). Global Proteomics Analysis of the Response to Starvation in C. elegans. Molecular & cellular proteomics : MCP *14*, 1989-2001.
Leon, I.R., Schwammle, V., Jensen, O.N., and Sprenger, R.R. (2013). Quantitative assessment of in-solution digestion efficiency identifies optimal protocols for unbiased protein analysis. Molecular & cellular proteomics : MCP *12*, 2992-3005.
Liang, V., Ullrich, M., Lam, H., Chew, Y.L., Banister, S., Song, X., Zaw, T., Kassiou, M., Gotz, J., and Nicholas, H.R. (2014). Altered proteostasis in aging and heat shock response in C. elegans revealed by analysis of the global and de novo synthesized proteome. Cellular and molecular life sciences : CMLS *71*, 3339-3361.
Liu, K., and Czaja, M.J. (2013). Regulation of lipid stores and metabolism by lipophagy. Cell Death Differ *20*, 3-11.
Longo, V.D., and Mattson, M.P. (2014). Fasting: molecular mechanisms and clinical applications. Cell metabolism *19*, 181-192.
Love, M.I., Huber, W., and Anders, S. (2014). Moderated estimation of fold change and dispersion for RNA-seq data with DESeq2. Genome Biol *15*, 550.
Ly, T., Ahmad, Y., Shlien, A., Soroka, D., Mills, A., Emanuele, M.J., Stratton, M.R., and Lamond, A.I. (2014). A proteomic chronology of gene expression through the cell cycle in human myeloid leukemia cells. Elife *3*, e01630.
Ma, X., Zhu, Y., Li, C., Xue, P., Zhao, Y., Chen, S., Yang, F., and Miao, L. (2014). Characterisation of Caenorhabditis elegans sperm transcriptome and proteome. BMC Genomics *15*, 168.
Magini, A., Polchi, A., Urbanelli, L., Cesselli, D., Beltrami, A., Tancini, B., and Emiliani, C. (2013). TFEB activation promotes the recruitment of lysosomal glycohydrolases beta-hexosaminidase and beta-galactosidase to the plasma membrane. Biochem Biophys Res Commun *440*, 251-257.

Maier, T., Schmidt, A., Guell, M., Kuhner, S., Gavin, A.C., Aebersold, R., and Serrano, L. (2011). Quantification of mRNA and protein and integration with protein turnover in a bacterium. Mol Syst Biol *7*, 511.
Murphy, C.T., McCarroll, S.A., Bargmann, C.I., Fraser, A., Kamath, R.S., Ahringer, J., Li, H., and Kenyon, C. (2003). Genes that act downstream of DAF-16 to influence the lifespan of Caenorhabditis elegans. Nature *424*, 277-283.
Murtagh, F., and Legendre, P. (2014). Ward's Hierarchical Agglomerative Clustering Method: Which Algorithms Implement Ward's Criterion? J Classif *31*, 274-295.
Narayan, V., Ly, T., Pourkarimi, E., Murillo, A.B., Gartner, A., Lamond, A.I., and Kenyon, C. (2016). Deep Proteome Analysis Identifies Age-Related Processes in C. elegans. Cell Syst.
Narbonne, P., and Roy, R. (2009). *Caenorhabditis elegans* dauers need LKB1/AMPK to ration lipid reserves and ensure long-term survival. Nature *457*, 210-214.
O'Rourke, E.J., and Ruvkun, G. (2013). MXL-3 and HLH-30 transcriptionally link lipolysis and autophagy to nutrient availability. Nat Cell Biol *15*, 668-676.
Pak, S.C., Kumar, V., Tsu, C., Luke, C.J., Askew, Y.S., Askew, D.J., Mills, D.R., Bromme, D., and Silverman, G.A. (2004). SRP-2 is a cross-class inhibitor that participates in postembryonic development of the nematode Caenorhabditis elegans: initial characterization of the clade L serpins. J Biol Chem *279*, 15448-15459.
Palgunow, D., Klapper, M., and Doring, F. (2012). Dietary restriction during development enlarges intestinal and hypodermal lipid droplets in Caenorhabditis elegans. PloS one *7*, e46198.
Pang, S., Lynn, D.A., Lo, J.Y., Paek, J., and Curran, S.P. (2014). SKN-1 and Nrf2 couples proline catabolism with lipid metabolism during nutrient deprivation. Nat Commun *5*, 5048.
Pena-Llopis, S., Vega-Rubin-de-Celis, S., Schwartz, J.C., Wolff, N.C., Tran, T.A., Zou, L., Xie, X.J., Corey, D.R., and Brugarolas, J. (2011). Regulation of TFEB and V-ATPases by mTORC1. The EMBO journal *30*, 3242-3258.
Roczniak-Ferguson, A., Petit, C.S., Froehlich, F., Qian, S., Ky, J., Angarola, B., Walther, T.C., and Ferguson, S.M. (2012). The transcription factor TFEB links mTORC1 signaling to transcriptional control of lysosome homeostasis. Science signaling *5*, ra42.
Schwammle, V., Leon, I.R., and Jensen, O.N. (2013). Assessment and improvement of statistical tools for comparative proteomics analysis of sparse data sets with few experimental replicates. J Proteome Res *12*, 3874-3883.
Seah, N.E., de Magalhaes Filho, C.D., Petrashen, A.P., Henderson, H.R., Laguer, J., Gonzalez, J., Dillin, A., Hansen, M., and Lapierre, L.R. (2016). Autophagy-mediated longevity is modulated by lipoprotein biogenesis. Autophagy *12*, 261-272.
Settembre, C., De Cegli, R., Mansueto, G., Saha, P.K., Vetrini, F., Visvikis, O., Huynh, T., Carissimo, A., Palmer, D., Klisch, T.J., et al. (2013). TFEB controls cellular lipid metabolism through a starvation-induced autoregulatory loop. Nature cell biology *15*, 647-658.
Settembre, C., Di Malta, C., Polito, V.A., Garcia Arencibia, M., Vetrini, F., Erdin, S., Erdin, S.U., Huynh, T., Medina, D., Colella, P., et al. (2011). TFEB links autophagy to lysosomal biogenesis. Science *332*, 1429-1433.
Silva, J.C., Gorenstein, M.V., Li, G.Z., Vissers, J.P., and Geromanos, S.J. (2006). Absolute quantification of proteins by LCMSE: a virtue of parallel MS acquisition. Molecular & cellular proteomics : MCP *5*, 144-156.
Simonsen, K.T., Gallego, S.F., Faergeman, N.J., and Kallipolitis, B.H. (2012). Strength in numbers: "Omics" studies of C. elegans innate immunity. Virulence *3*, 477-484.
Spivak, M., Weston, J., Bottou, L., Kall, L., and Noble, W.S. (2009). Improvements to the percolator algorithm for Peptide identification from shotgun proteomics data sets. J Proteome Res *8*, 3737-3745.
Tetlak, A.G., Burnett, J.B., Hahn, D.A., and Hatle, J.D. (2015). Vitellogenin-RNAi and ovariectomy each increase lifespan, increase protein storage, and decrease feeding, but are not additive in grasshoppers. Biogerontology *16*, 761-774.

Van Gilst, M.R., Hadjivassiliou, H., and Yamamoto, K.R. (2005). A Caenorhabditis elegans nutrient response system partially dependent on nuclear receptor NHR-49. Proceedings of the National Academy of Sciences of the United States of America *102*, 13496-13501.
Van Rompay, L., Borghgraef, C., Beets, I., Caers, J., and Temmerman, L. (2015). New genetic regulators question relevance of abundant yolk protein production in C. elegans. Sci Rep *5*, 16381.
Visvikis, O., Ihuegbu, N., Labed, S.A., Luhachack, L.G., Alves, A.M., Wollenberg, A.C., Stuart, L.M., Stormo, G.D., and Irazoqui, J.E. (2014). Innate Host Defense Requires TFEB-Mediated Transcription of Cytoprotective and Antimicrobial Genes. Immunity *40*, 896-909.
Vogel, C., and Marcotte, E.M. (2012). Insights into the regulation of protein abundance from proteomic and transcriptomic analyses. Nat Rev Genet *13*, 227-232.
Walther, D.M., Kasturi, P., Zheng, M., Pinkert, S., Vecchi, G., Ciryam, P., Morimoto, R.I., Dobson, C.M., Vendruscolo, M., Mann, M., et al. (2015). Widespread Proteome Remodeling and Aggregation in Aging C. elegans. Cell *161*, 919-932.
Wang, W., Gao, Q., Yang, M., Zhang, X., Yu, L., Lawas, M., Li, X., Bryant-Genevier, M., Southall, N.T., Marugan, J., et al. (2015). Up-regulation of lysosomal TRPML1 channels is essential for lysosomal adaptation to nutrient starvation. Proceedings of the National Academy of Sciences of the United States of America *112*, E1373-1381.
Wilkins, M.R., Gasteiger, E., Bairoch, A., Sanchez, J.C., Williams, K.L., Appel, R.D., and Hochstrasser, D.F. (1999). Protein identification and analysis tools in the ExPASy server. Methods Mol Biol *112*, 531-552.
Yang, W., Dierking, K., Esser, D., Tholey, A., Leippe, M., Rosenstiel, P., and Schulenburg, H. (2015). Overlapping and unique signatures in the proteomic and transcriptomic responses of the nematode Caenorhabditis elegans toward pathogenic Bacillus thuringiensis. Dev Comp Immunol *51*, 1-9.
Zhang, J., Bakheet, R., Parhar, R.S., Huang, C.H., Hussain, M.M., Pan, X., Siddiqui, S.S., and Hashmi, S. (2011). Regulation of fat storage and reproduction by Kruppel-like transcription factor KLF3 and fat-associated genes in Caenorhabditis elegans. J Mol Biol *411*, 537-553.
Zhang, Y., Zou, X., Ding, Y., Wang, H., Wu, X., and Liang, B. (2013). Comparative genomics and functional study of lipid metabolic genes in Caenorhabditis elegans. BMC Genomics *14*, 164.
Zimmerman, S.M., Hinkson, I.V., Elias, J.E., and Kim, S.K. (2015). Reproductive Aging Drives Protein Accumulation in the Uterus and Limits Lifespan in C. elegans. PLoS Genet *11*, e1005725.

Strain	RNAi treament	RNAi survival-span (d)	Number of RNAi animals	Control survival-span (d)	Number of Control animals	Max survival-span	*p*-value versus Control
N2	*vit-1*	7	89/120	7	78/108	9/10	0.9032
	vit-1	7	82/120	8	85/108	9/10	0.0186
	vit-1	5	69/120	6	88/120	9/10	0.0990
	vit-5	7	85/120	7	78/108	9/10	0.8806
	vit-5	7	69/108	8	85/108	10/10	0.5453
	vit-5	5	88/120	6	88/120	9/10	0.1369
	ssq-4	5	68/120	5	83/120	9/10	0.2839
	ssq-4	7	81/120	6	91/120	10/10	0.5187
	ssq-4	6	97/120	7	90/120	10/10	0.0156
	unc-41	6	88/108	7	77/108	10/10	0.1885
	unc-41	7	77/108	6	91/120	10/10	0.5584
	unc-41	6	95/120	7	90/120	10/10	0.0029
JIN1375 (*hlh-30)*	*vit-1*	7	93/120	5	79/120	9/8	<0.0001
	vit-1	7	81/120	5	89/120	9/7	<0.0001
	vit-1	6	83/120	5	73/108	9/7	<0.0001
	vit-5	7	82/120	5	79/120	9/8	<0.0001
	vit-5	6	88/120	5	89/120	9/7	0.0003
	vit-5	5	83/120	5	73/108	9/7	0.0004
	ssq-4	6	72/120	4	70/120	9/6	<0.0001
	ssq-4	5	85/120	5	85/120	10/7	0.0045
	ssq-4	6	80/120	5	79/120	10/7	<0.0001
	unc-41	7	78/120	5	84/120	9/7	<0.0001
	unc-41	6	85/120	5	85/120	10/7	<0.0001
	unc-41	7	76/108	5	79/120	10/7	<0.0001

Table 1 Log-rank statistical analyses of starvation survival rates. Mean- and max survival and statistical significance were calculated for each experiment as detailed in Materials and Methods. All experiments were carried out in triplicates, each comprising 9 or 10 plates with 12 animals on each.

Figure legends

Figure 1 Work-flow for label-free quantitative proteomics of starvation responses in *C. elegans*. A. *C. elegans* (N2 Bristol and the *hlh-30* mutant TM1978) were starved at the mid-L4 larvae state for the time indicated and harvested for 2D-label-free proteomics and RNA-seq. For proteomics, proteins were extracted and digested with trypsin, and the resulting peptides were analyzed by 2D LC-MS/MS label-free quantitative proteomics. For RNA-seq total RNA was extracted and after polyA selection cDNA was prepared and analyzed by deep sequencing. B. Venn diagram showing the number of identified proteins in wild type animals and *hlh-30* animals for the three biological replicates at each time point. The numbers of proteins detected with at least two peptides are indicated. C. Protein density plots showing the distribution of $\log_2$ ratios for each time point relative to the fed state for each both wild type animals and *hlh-30* animals. The plots are based on the mean of the triplicates for each time point for ~4,400 identified proteins. D. Volcano plot of the identified proteins for each time point and for both wild type and *hlh-30* mutant animals. Each point represents the difference in expression (fold-change) relative to fed animals (time = 0) plotted against the level of statistical significance. The plots are based on the mean of the triplicates for each time point for ~4,400 identified proteins. The color intensity indicates the density of data points.

Figure 2 Temporal profiling of starvation responses reveal early and late responses in proteomes. A. Heat map illustrating the temporal changes between fed wild type *C. elegans* and wild type *C. elegans* starved for 1, 2, 3, 4, 6, and 16 hours. Only proteins (1,780) that were significantly changed (q-value ≤0.05) at at least one time point, are depicted. Data were scaled across rows before mapping to colors. B. Dot plots of enriched KEGG pathways. Enrichment of KEGG pathways among the proteins in each of the 4 clusters shown in (A). The x-axis shows the fold enrichment of each KEGG pathway, whereas the color denotes the p-value and the size of the dot denotes the number of IDs assigned to each KEGG pathway.

Figure 3 Transcriptome profiling of starvation responses in *C. elegans* reveals a poor correlation between RNA and protein levels. A. Venn diagram showing the number of identified RNAs in wild type animals and *hlh-30* animals for the three biological replicates at each time point. B. Volcano plot of the identified mRNAs for each time point and for both wild type and *hlh-30* mutant animals. Each point represents the abundance of a given mRNA relative to the fed animals (log_2 ratio) at time point 0 plotted against the level of statistical significance. The plots are based on the mean of the triplicates for each time point for ~10,700 identified genes. The color indicates the density of data points. C. Correlation of log-transformed protein intensities and log-transformed FPKM values (RNA intensities) from wild type animals and *hlh-30* animals for each time point. Each graph is annotated with the calculated Spearmen correlation coefficients (r).

Figure 4 Comparison and functional annotation of starvation-induced changes in protein and RNA abundance. A. Heat map illustrating the temporal changes in protein and RNA between fed wild type *C. elegans* and wild type *C. elegans* in response to starvation for 1, 2, 3, 4, 6, and 16 hours. Only proteins (2,750) and their corresponding RNAs that were identified at all time points are depicted. Data were scaled across rows before mapping to colors. B. Dot plots of enriched KEGG pathways in the four clusters shown in (A). The x-axis shows the fold enrichment of each KEGG pathway, whereas the color denotes the p-value and the size of the dot denotes the number of IDs assigned to each KEGG pathway.

Figure 5 Proteome profiling of starvation responses in *hlh-30* animals identifies novel functions of HLH-30 in *C. elegans*. A. The score plotted as *A* (1-(Absolute correlation coefficient)) versus *B* (integrated difference between the curves). The coordinates of known HLH-30 targets are marked with the protein name in red. The color indicates the density of data points. B. Dot plots of enriched KEGG pathways among the proteins with a score above the 75th percentile. The x-axis shows the fold enrichment of each pathway, whereas the color denotes the p-value and the size of the dot denotes the count (number of IDs assigned to each KEGG pathway). Only GO terms with p-value < 0.05 are plotted. C. Dot plots of enriched GO terms

among the proteins with a score above the 75th percentile. The x-axis shows the fold enrichment of each GO term, whereas the color denotes the p-value and the size of the dot denotes the count (number of IDs assigned to each GO term). D. Dot plots of enriched GO terms among the RNA with a score above the 75th percentile. The x-axis shows the fold enrichment of each GO term, whereas the color denotes the p-value and the size of the dot denotes the count (number of IDs assigned to each GO term).

Figure 6 Knock down of vitellogenins improves survival of *hlh-30* animals in response to acute starvation. Effects of RNAi mediated knock down of vitellogenins on starvation survival. Wild type or *hlh-30* animals were subjected to RNAi against *vit-1* (A), *vit-5* (B), *ssq-4* (C), *unc-41* (D) or control (L4440 empty vector) and subsequently starved at 20°C. Statistical analyses of data shown are reported in Table 1.

Figure 7 Knock-down of vitellogenin 1 affetcs number and size of intestinal lipid droplets in *hlh-30 animals* but not in wild type animals. Intestinal lipid droplets were visulalized by Coherent Anti-Stokes Raman Scattering microscopy and size and number of lipid droplets were determined by DropletFinder in ImageJ. The distribution of the lipid droplet size in both wild type animals and *hlh-30* animals was determined in fed animals and in animals starved for 3, 6, and 8 hours) subjected to either control RNAi or RNAi against *vit-1*. An overlay of all conditions is shown in the last column.

Supplemental information

Figure S1 Ranked plots for protein abundance based on the mean value derived from the triplicates for each time point in both genetic backgrounds.

Figure S2 Matrix representation of Pearson correlation values of the label-free protein abundances of each replicate against the others for both wild type animals (A) and hlh-30 animals (B).

Correlations are uniformly high for early time points, varying only between r = 0.92 and 0.98. Correlations are indicated in the color gradient to the right of each plot.

Figure S3 Volcano plot of the identified proteins after 16 hours starvation for both wild type animals. Each point represents the difference in expression (fold-change) relative to fed animals (time = 0) plotted against the level of statistical significance. Proteins that previously have been found regulated by starvation have been highlighted.

Figure S4 Dot plot of enriched GO terms for up- (A) and down-regulated (B) proteins in wild type animals, respectively. The x-axis indicates the duration of starvation, whereas the color represents enrichment and the size depicts –log10(p-value) of each GO term.

Figure S5 Pie diagrams visualizing the percentage of genes encoded in each chromosome in *C. elegans* identified in the present study (A) and according to The *C. elegans* Sequencing Consortium 1998 (B).

Figure S6 Number of significantly up- (blue) or down- (red) regulated proteins and mRNAs at each time point in wild type animals.

Figure S7 Protein and mRNA abundance of FAT-1/*fat-1*, FAT-2/*fat-2*, FAT-4/*fat-4* and FAT-6/*fat-6* in wild type (turquoise) and in *hlh-30* animals (red). Protein and mRNA abundances are shown in fmol/μg and RPKM, respectively.

Figure S8 Dot plot of enriched GO terms for up- (A) and down-regulated (B) mRNAs in wild type animals, respectively. The x-axis indicates the duration of starvation, whereas the color represents enrichment and the size depicts –log10(p-value) of each GO term.

Figure S9 A. Examples of known HLH-30 regulated proteins plotted as line graphs as $\log_2$ transformed protein ratios relative to wild type fed (t = 0). The correlation and the absolute integrated area between the curve representing protein ratio for wild type and mutant are indicated for each protein in the plot. Graph representing wild type animals and *hlh-30* animals is shown in

turquoise and red, respectively. B. The absolute integral shown as density plot. The integral is plotted on the y-axis and the density on the x-axis. The value of the absolute integral for known HLH-30 regulated genes is shown in red lines and indicated by the protein name. New potential targets identified using the score are indicated in red with a dashed line.

Figure S10 Box plots including Turkey's Five numbers for proteins according to the score (A) or the absolute integral score (B). Proteins above the upper-hinge (1.85) were considered of interest.

Figure S11 Protein- and mRNA abundances of vitellogenins in fed wild type animals and hlh-30 animals plotted as line graphs as $\log_2$ transformed protein ratios relative to time point 0. Graph representing wild type animals and *hlh-30* animals is shown in turquoise and red nuances, respectively.

Figure 1

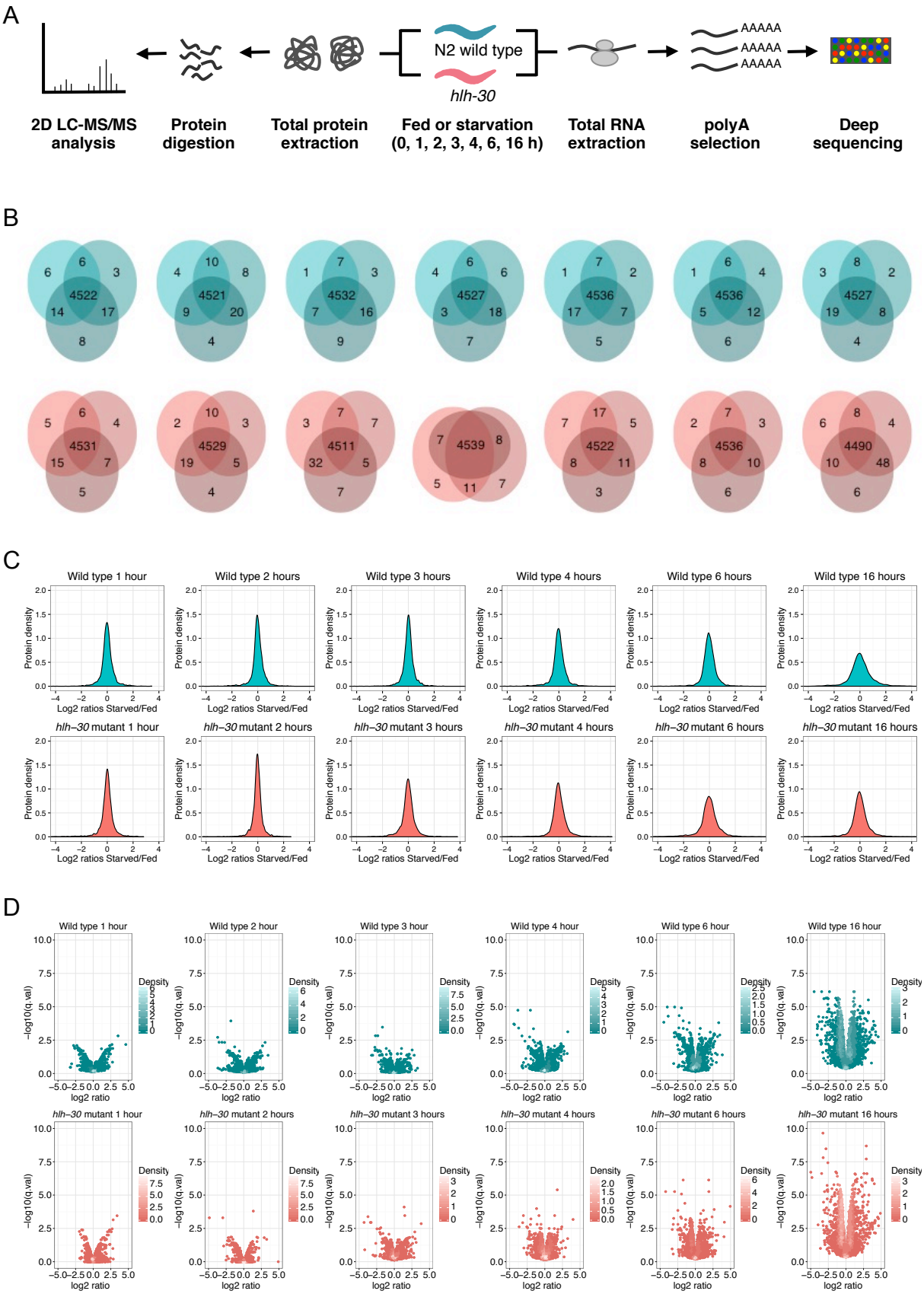
A
N2 wild type
hlh-30
AAAAA
AAAAA
AAAAA
2D LC-MS/MS analysis
Protein digestion
Total protein extraction
Fed or starvation (0, 1, 2, 3, 4, 6, 16 h)
Total RNA extraction
polyA selection
Deep sequencing
B
6 6 3 4522 14 17 8
4 10 8 4521 9 20 4
1 7 3 4532 7 16 9
4 6 6 4527 3 18 7
1 7 2 4536 17 7 5
1 6 4 4536 5 12 6
3 8 2 4527 19 8 4
5 6 4 4531 15 7 5
2 10 3 4529 19 5 4
3 7 7 4511 32 5 7
7 4539 8 5 11 7
7 17 5 4522 8 11 3
2 7 3 4536 8 10 6
6 8 4 4490 10 48 6
C
Wild type 1 hour
Wild type 2 hours
Wild type 3 hours
Wild type 4 hours
Wild type 6 hours
Wild type 16 hours
hlh–30 mutant 1 hour
hlh–30 mutant 2 hours
hlh–30 mutant 3 hours
hlh–30 mutant 4 hours
hlh–30 mutant 6 hours
hlh–30 mutant 16 hours
Protein density
Log2 ratios Starved/Fed
D
Wild type 1 hour
Wild type 2 hour
Wild type 3 hour
Wild type 4 hour
Wild type 6 hour
Wild type 16 hour
hlh–30 mutant 1 hour
hlh–30 mutant 2 hours
hlh–30 mutant 3 hours
hlh–30 mutant 4 hours
hlh–30 mutant 6 hours
hlh–30 mutant 16 hours
−log10(q.val)
log2 ratio
Density

Figure 2

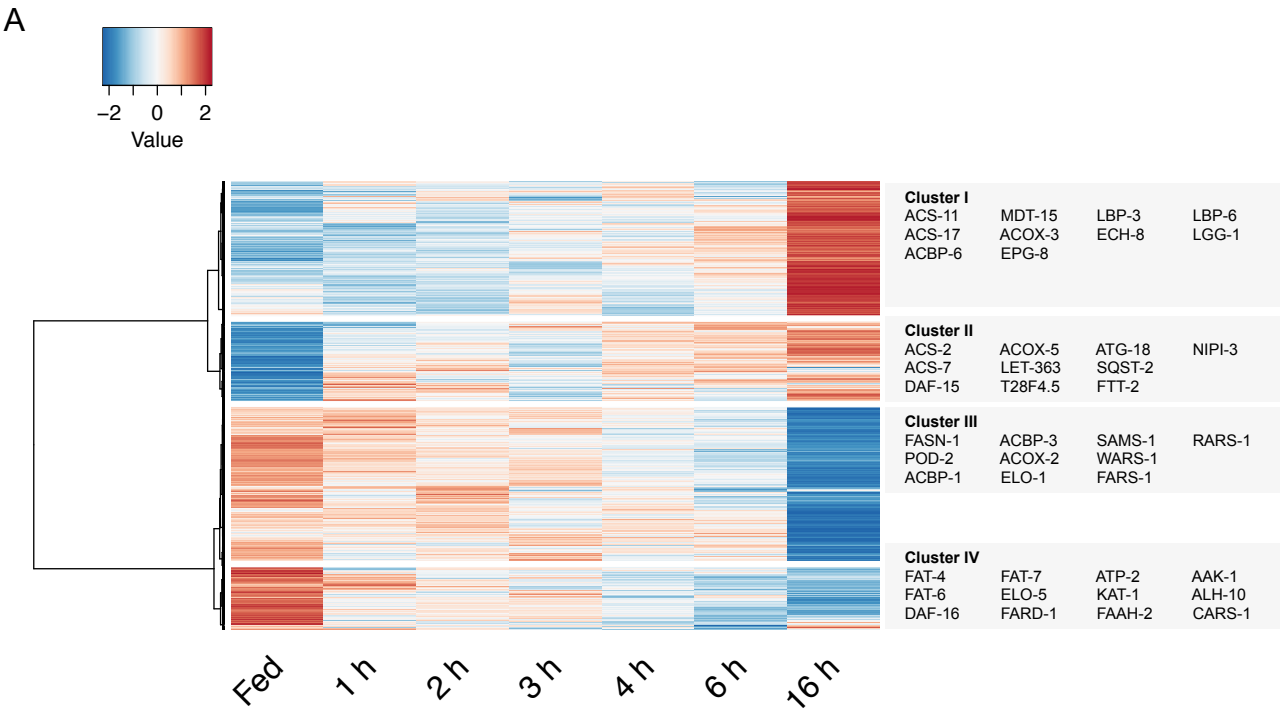
A
−2
0
2
Value
Cluster I
ACS-11 MDT-15 LBP-3 LBP-6
ACS-17 ACOX-3 ECH-8 LGG-1
ACBP-6 EPG-8
Cluster II
ACS-2 ACOX-5 ATG-18 NIPI-3
ACS-7 LET-363 SQST-2
DAF-15 T28F4.5 FTT-2
Cluster III
FASN-1 ACBP-3 SAMS-1 RARS-1
POD-2 ACOX-2 WARS-1
ACBP-1 ELO-1 FARS-1
Cluster IV
FAT-4 FAT-7 ATP-2 AAK-1
FAT-6 ELO-5 KAT-1 ALH-10
DAF-16 FARD-1 FAAH-2 CARS-1
Fed
1 h
2 h
3 h
4 h
6 h
16 h

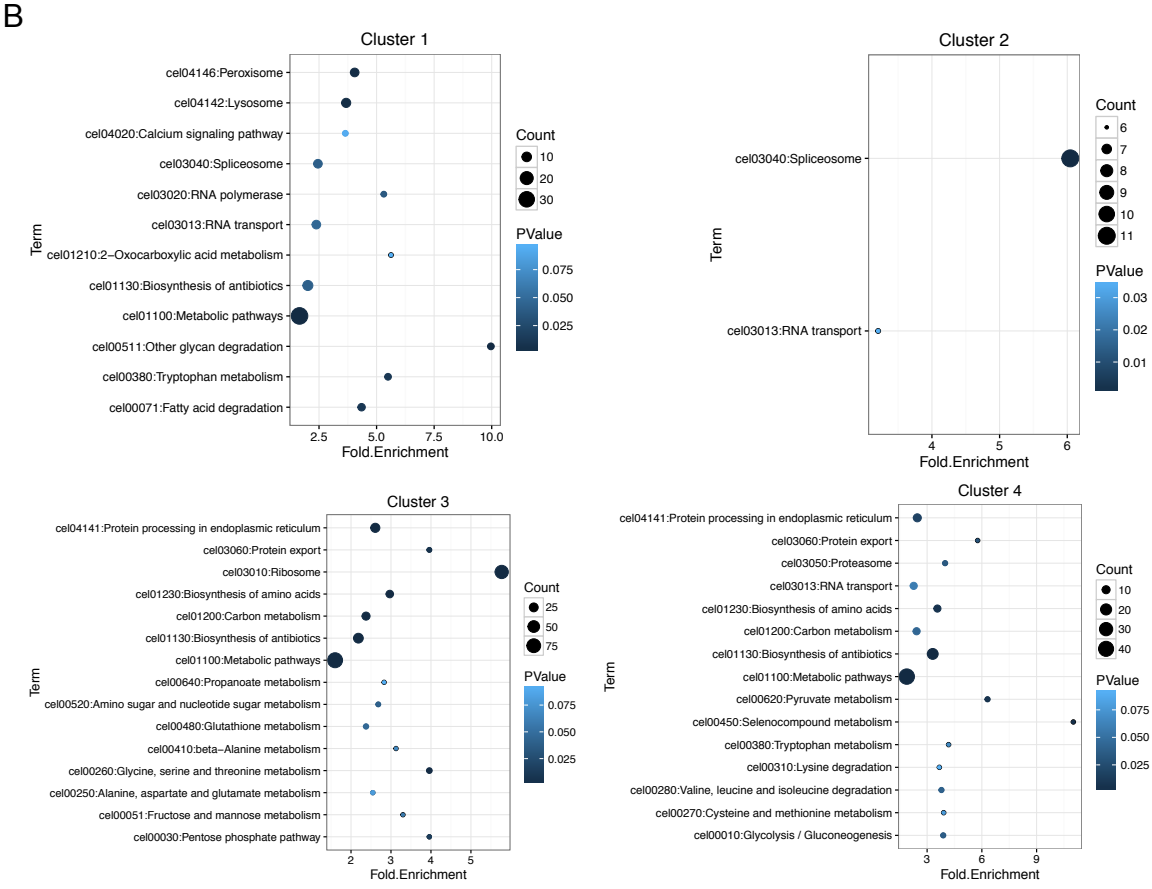
B
Cluster 1
cel04146:Peroxisome
cel04142:Lysosome
cel04020:Calcium signaling pathway
cel03040:Spliceosome
cel03020:RNA polymerase
cel03013:RNA transport
cel01210:2−Oxocarboxylic acid metabolism
cel01130:Biosynthesis of antibiotics
cel01100:Metabolic pathways
cel00511:Other glycan degradation
cel00380:Tryptophan metabolism
cel00071:Fatty acid degradation
Term
2.5 5.0 7.5 10.0
Fold.Enrichment
Count
10
20
30
PValue
0.075
0.050
0.025
Cluster 2
cel03040:Spliceosome
cel03013:RNA transport
Term
4 5 6
Fold.Enrichment
Count
6
7
8
9
10
11
PValue
0.03
0.02
0.01
Cluster 3
cel04141:Protein processing in endoplasmic reticulum
cel03060:Protein export
cel03010:Ribosome
cel01230:Biosynthesis of amino acids
cel01200:Carbon metabolism
cel01130:Biosynthesis of antibiotics
cel01100:Metabolic pathways
cel00640:Propanoate metabolism
cel00520:Amino sugar and nucleotide sugar metabolism
cel00480:Glutathione metabolism
cel00410:beta−Alanine metabolism
cel00260:Glycine, serine and threonine metabolism
cel00250:Alanine, aspartate and glutamate metabolism
cel00051:Fructose and mannose metabolism
cel00030:Pentose phosphate pathway
Term
2 3 4 5
Fold.Enrichment
Count
25
50
75
PValue
0.075
0.050
0.025
Cluster 4
cel04141:Protein processing in endoplasmic reticulum
cel03060:Protein export
cel03050:Proteasome
cel03013:RNA transport
cel01230:Biosynthesis of amino acids
cel01200:Carbon metabolism
cel01130:Biosynthesis of antibiotics
cel01100:Metabolic pathways
cel00620:Pyruvate metabolism
cel00450:Selenocompound metabolism
cel00380:Tryptophan metabolism
cel00310:Lysine degradation
cel00280:Valine, leucine and isoleucine degradation
cel00270:Cysteine and methionine metabolism
cel00010:Glycolysis / Gluconeogenesis
Term
3 6 9
Fold.Enrichment
Count
10
20
30
40
PValue
0.075
0.050
0.025

Figure 3

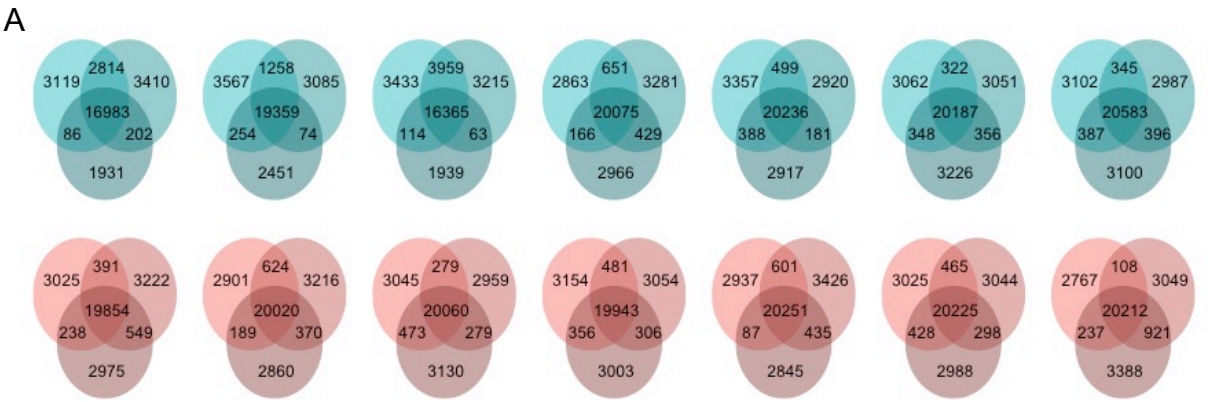
A
3119 2814 3410 16983 86 202 1931
3567 1258 3085 19359 254 74 2451
3433 3959 3215 16365 114 63 1939
2863 651 3281 20075 166 429 2966
3357 499 2920 20236 388 181 2917
3062 322 3051 20187 348 356 3226
3102 345 2987 20583 387 396 3100
3025 391 3222 19854 238 549 2975
2901 624 3216 20020 189 370 2860
3045 279 2959 20060 473 279 3130
3154 481 3054 19943 356 306 3003
2937 601 3426 20251 87 435 2845
3025 465 3044 20225 428 298 2988
2767 108 3049 20212 237 921 3388

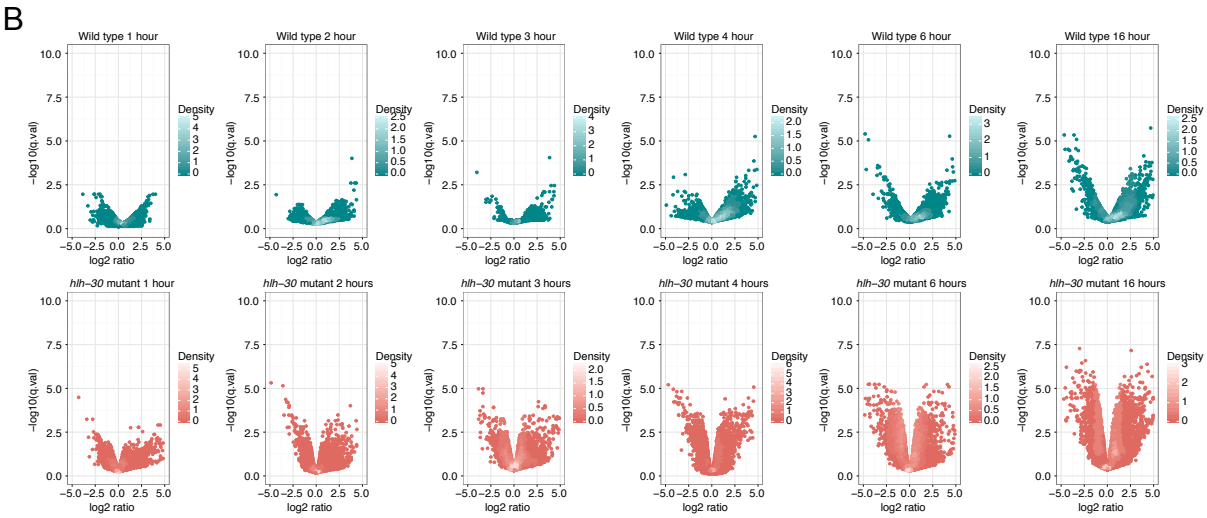
B
Wild type 1 hour
Wild type 2 hour
Wild type 3 hour
Wild type 4 hour
Wild type 6 hour
Wild type 16 hour
hlh-30 mutant 1 hour
hlh-30 mutant 2 hours
hlh-30 mutant 3 hours
hlh-30 mutant 4 hours
hlh-30 mutant 6 hours
hlh-30 mutant 16 hours
−log10(q.val)
log2 ratio
Density

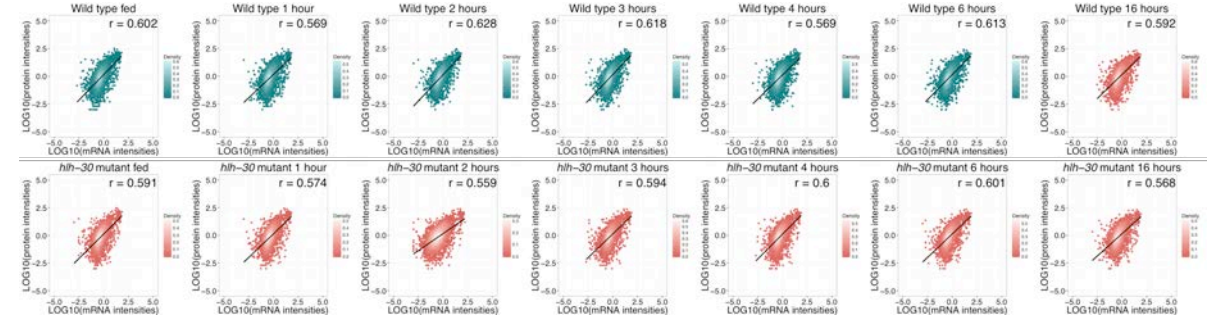
C
Wild type fed r = 0.602
Wild type 1 hour r = 0.569
Wild type 2 hours r = 0.628
Wild type 3 hours r = 0.618
Wild type 4 hours r = 0.569
Wild type 6 hours r = 0.613
Wild type 16 hours r = 0.592
hlh-30 mutant fed r = 0.591
hlh-30 mutant 1 hour r = 0.574
hlh-30 mutant 2 hours r = 0.559
hlh-30 mutant 3 hours r = 0.594
hlh-30 mutant 4 hours r = 0.6
hlh-30 mutant 6 hours r = 0.601
hlh-30 mutant 16 hours r = 0.568
LOG10(protein intensities)
LOG10(mRNA intensities)

Figure 4

A

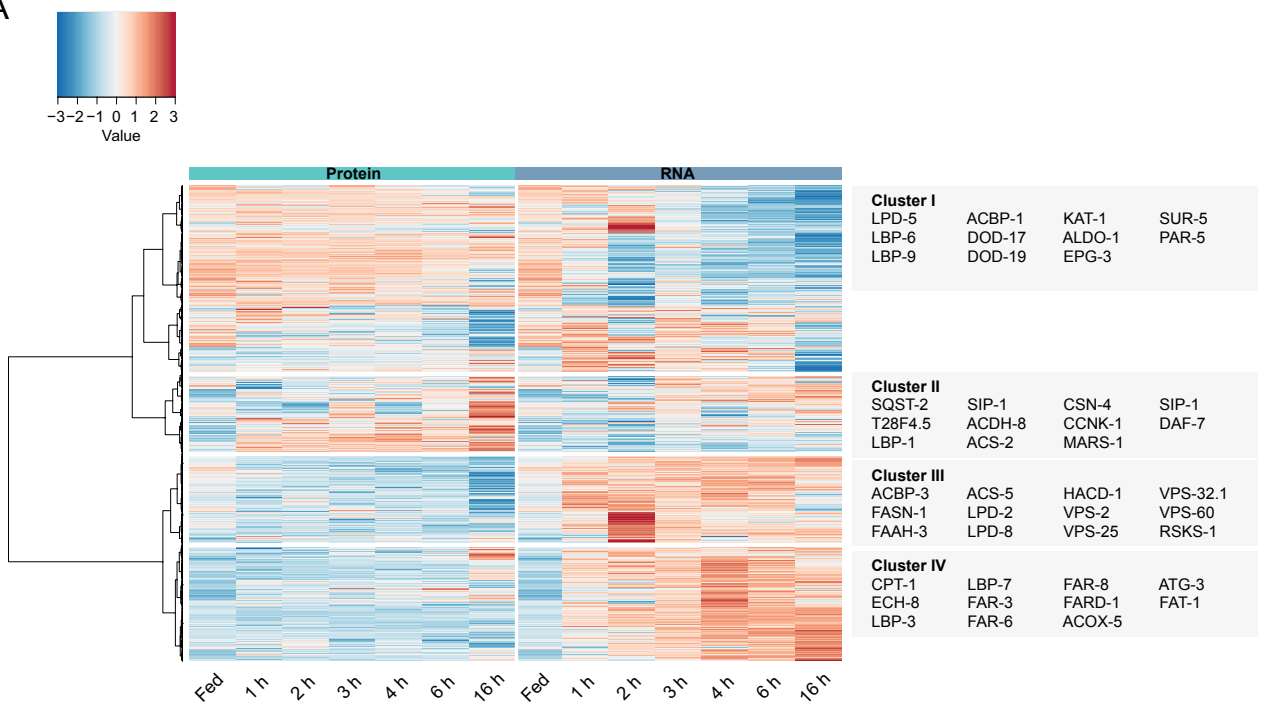

Cluster I

LPD-5	ACBP-1	KAT-1	SUR-5
LBP-6	DOD-17	ALDO-1	PAR-5
LBP-9	DOD-19	EPG-3	

Cluster II

SQST-2	SIP-1	CSN-4	SIP-1
T28F4.5	ACDH-8	CCNK-1	DAF-7
LBP-1	ACS-2	MARS-1	

Cluster III

ACBP-3	ACS-5	HACD-1	VPS-32.1
FASN-1	LPD-2	VPS-2	VPS-60
FAAH-3	LPD-8	VPS-25	RSKS-1

Cluster IV

CPT-1	LBP-7	FAR-8	ATG-3
ECH-8	FAR-3	FARD-1	FAT-1
LBP-3	FAR-6	ACOX-5	

B

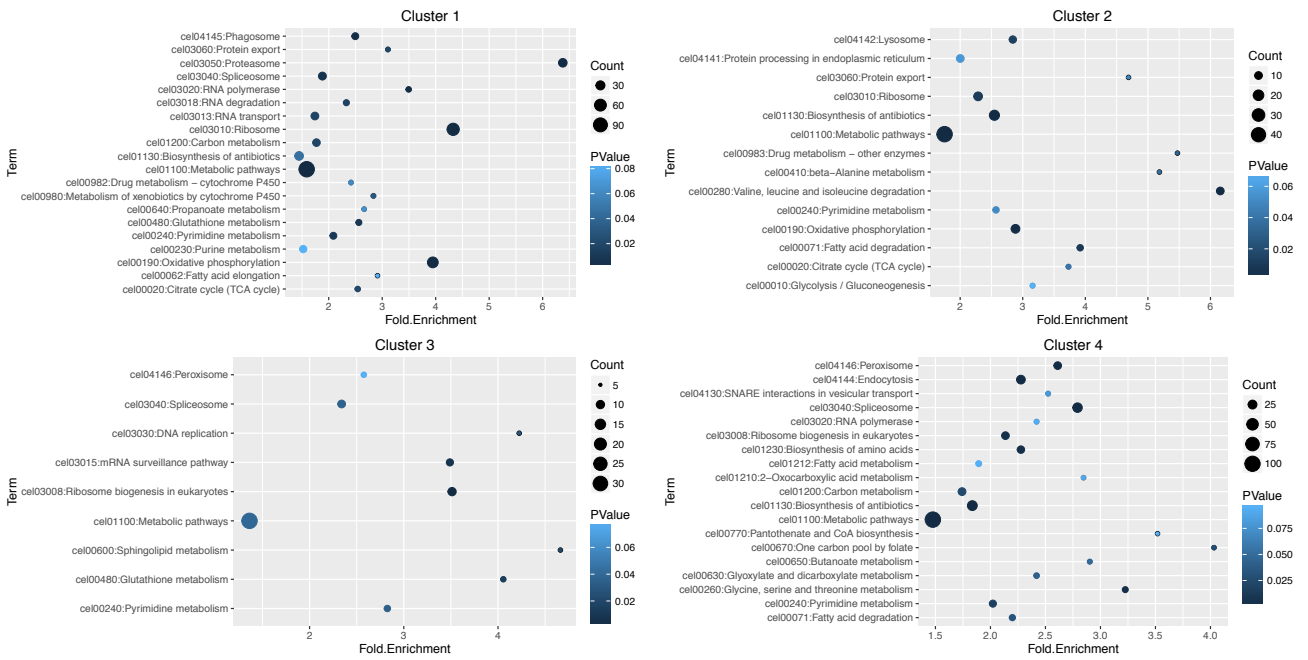

Figure 5

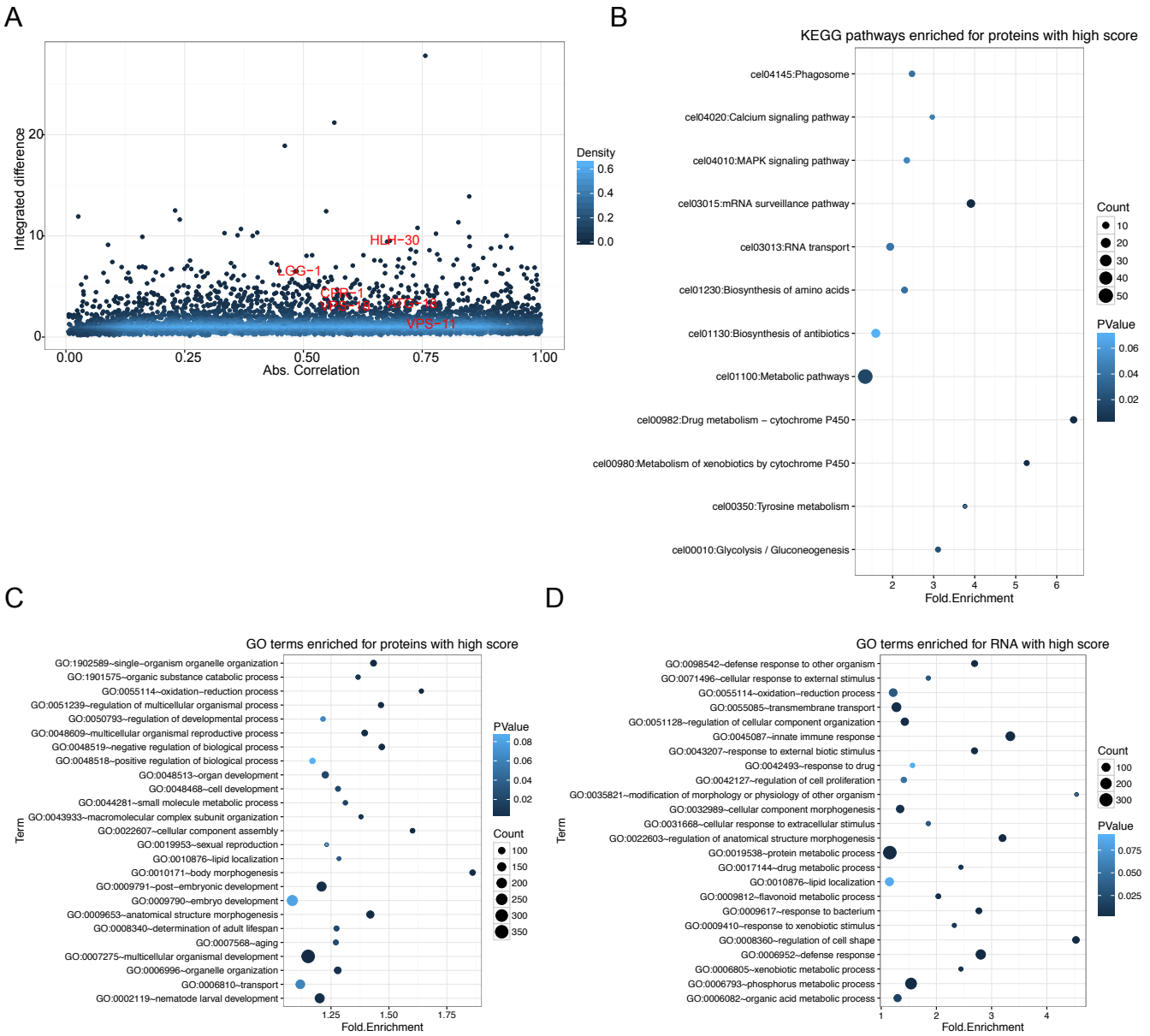
A
Integrated difference
Abs. Correlation
Density
LGG-1
HLH-30
CBP-1
VPS-11
B
KEGG pathways enriched for proteins with high score
cel04145:Phagosome
cel04020:Calcium signaling pathway
cel04010:MAPK signaling pathway
cel03015:mRNA surveillance pathway
cel03013:RNA transport
cel01230:Biosynthesis of amino acids
cel01130:Biosynthesis of antibiotics
cel01100:Metabolic pathways
cel00982:Drug metabolism – cytochrome P450
cel00980:Metabolism of xenobiotics by cytochrome P450
cel00350:Tyrosine metabolism
cel00010:Glycolysis / Gluconeogenesis
Fold.Enrichment
Count
PValue
C
GO terms enriched for proteins with high score
Term
Fold.Enrichment
Count
PValue
D
GO terms enriched for RNA with high score
Term
Fold.Enrichment
Count
PValue

Figure 6

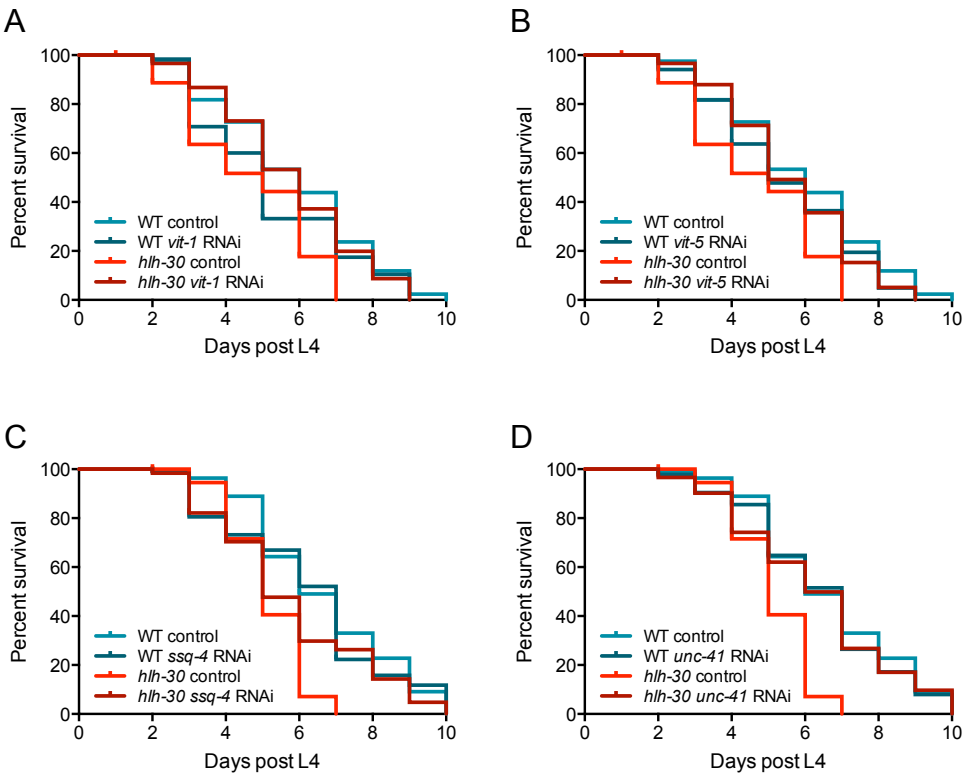
A
Percent survival
Days post L4
WT control
WT vit-1 RNAi
hlh-30 control
hlh-30 vit-1 RNAi
B
Percent survival
Days post L4
WT control
WT vit-5 RNAi
hlh-30 control
hlh-30 vit-5 RNAi
C
Percent survival
Days post L4
WT control
WT ssq-4 RNAi
hlh-30 control
hlh-30 ssq-4 RNAi
D
Percent survival
Days post L4
WT control
WT unc-41 RNAi
hlh-30 control
hlh-30 unc-41 RNAi

Figure 7

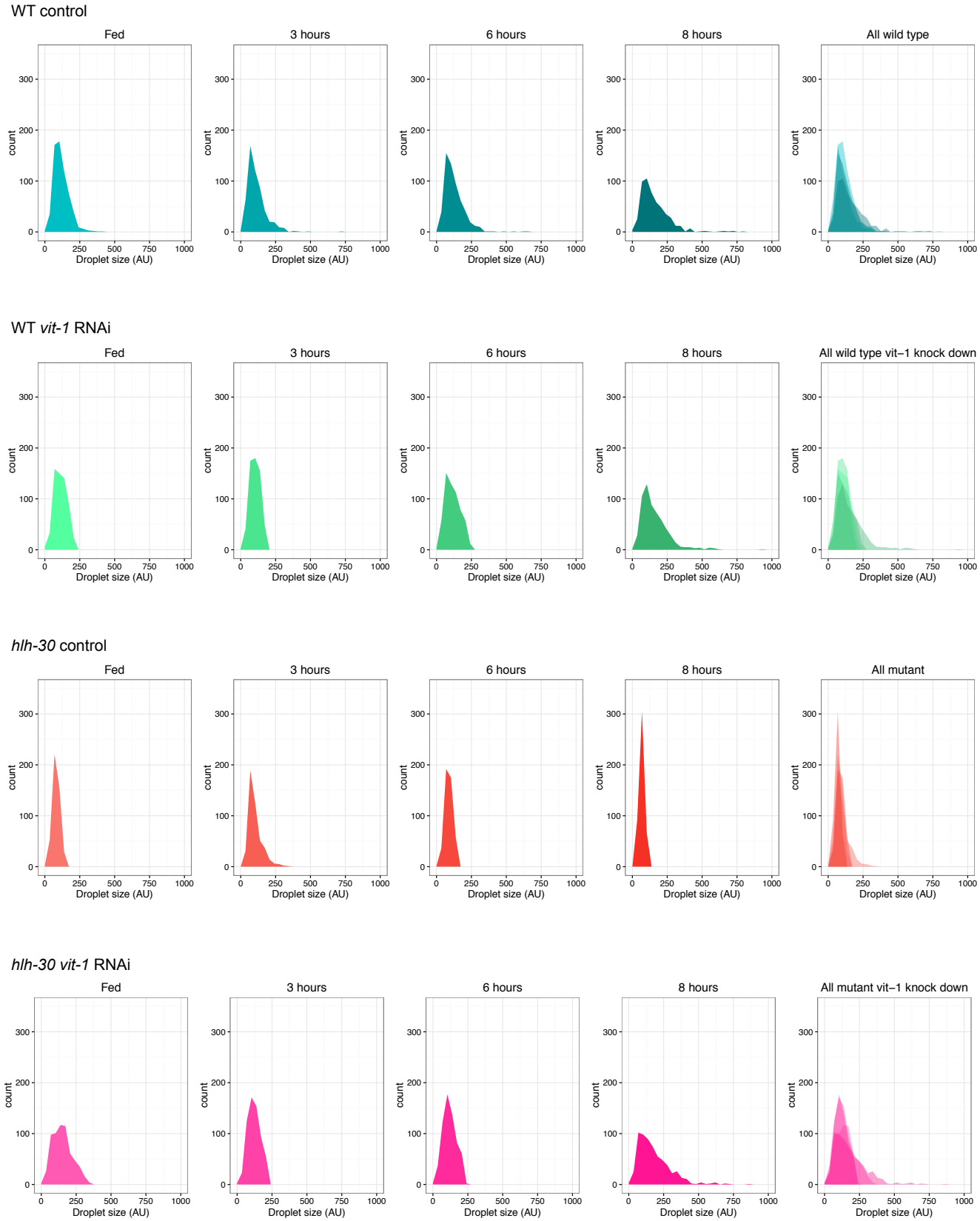
WT control
Fed
3 hours
6 hours
8 hours
All wild type
WT vit-1 RNAi
All wild type vit−1 knock down
hlh-30 control
All mutant
hlh-30 vit-1 RNAi
All mutant vit−1 knock down
count
Droplet size (AU)

Figure S1

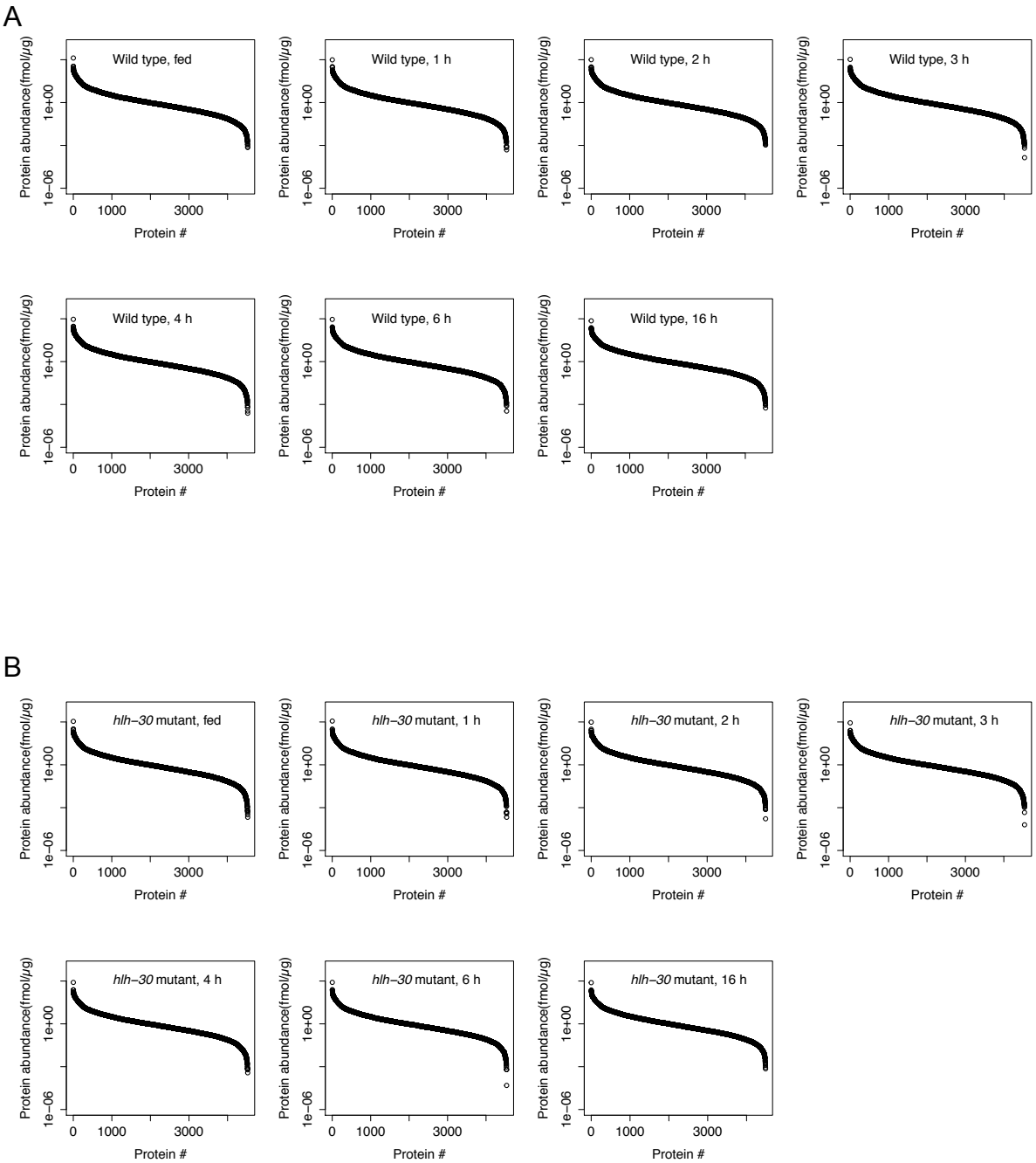
A
Wild type, fed
Wild type, 1 h
Wild type, 2 h
Wild type, 3 h
Wild type, 4 h
Wild type, 6 h
Wild type, 16 h
B
hlh–30 mutant, fed
hlh–30 mutant, 1 h
hlh–30 mutant, 2 h
hlh–30 mutant, 3 h
hlh–30 mutant, 4 h
hlh–30 mutant, 6 h
hlh–30 mutant, 16 h
Protein abundance(fmol/µg)
1e−06
1e+00
0
1000
3000
Protein #

Figure S2

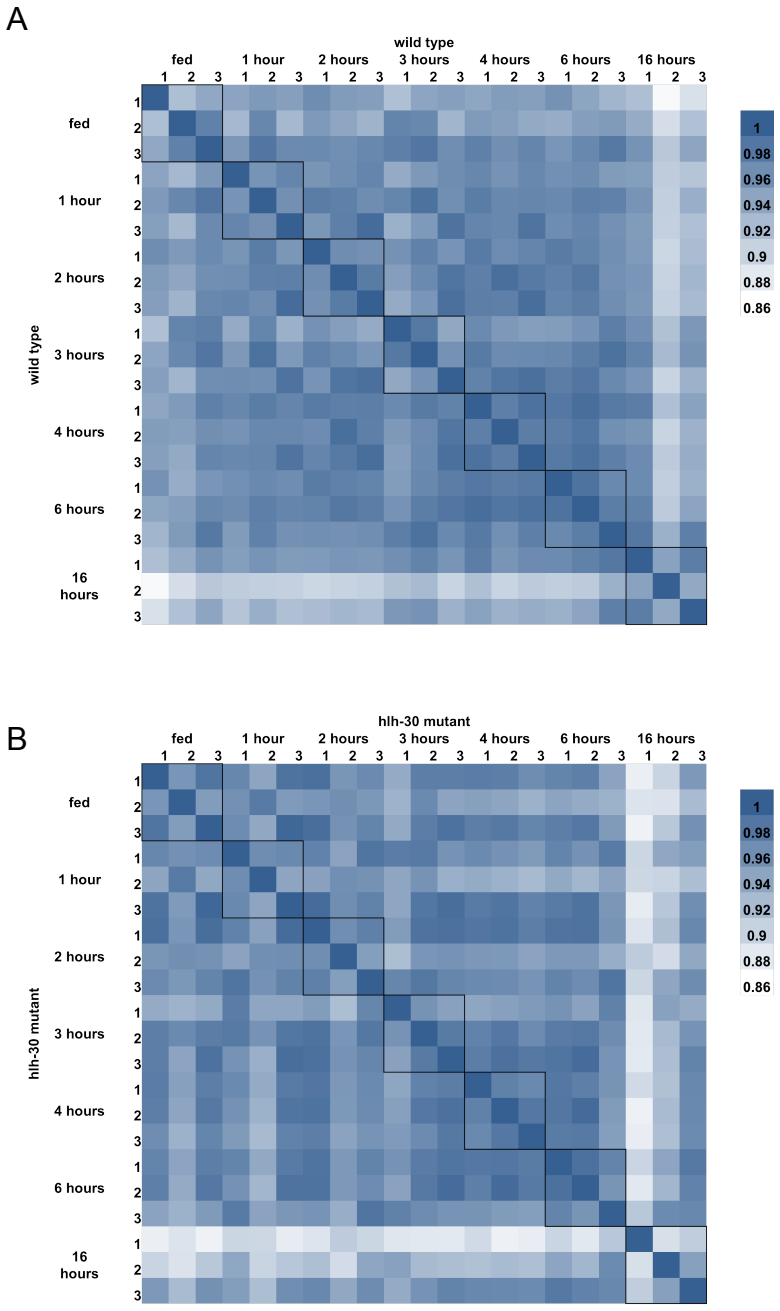
A
wild type
fed
1 hour
2 hours
3 hours
4 hours
6 hours
16 hours
1 2 3
wild type
1
0.98
0.96
0.94
0.92
0.9
0.88
0.86
B
hlh-30 mutant
hlh-30 mutant

Figure S3

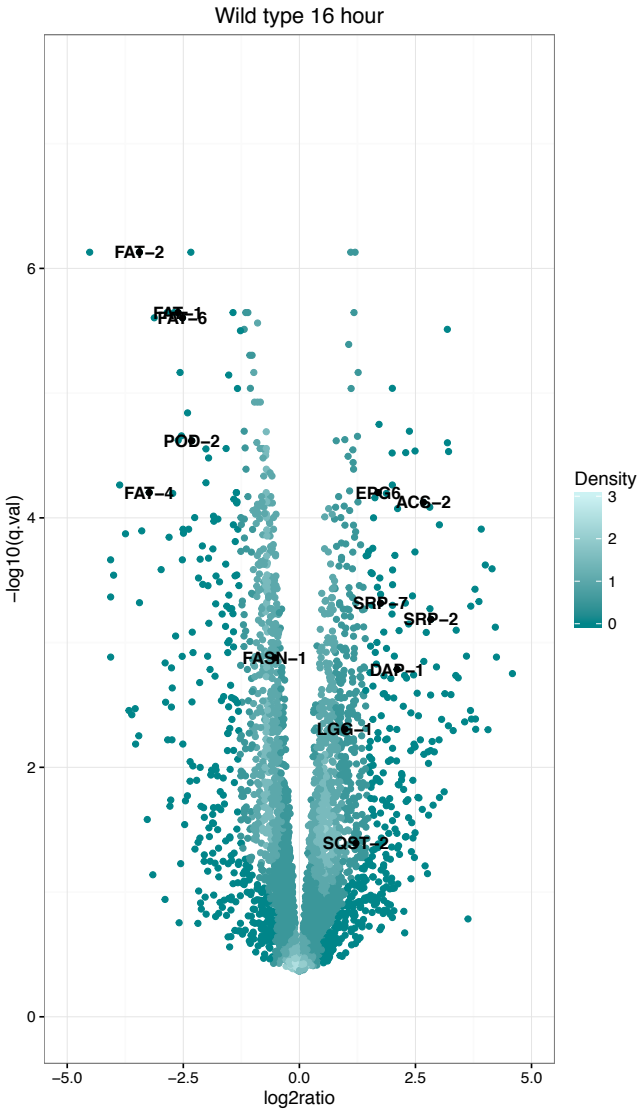
Wild type 16 hour
FAT−2
FAT−1
FAT−6
POD−2
FAT−4
EPG6
ACS−2
SRP−7
SRP−2
FASN−1
DAP−1
LGG−1
SQST−2
Density
3
2
1
0
6
4
2
0
−log10(q.val)
−5.0
−2.5
0.0
2.5
5.0
log2ratio

Figure S4A

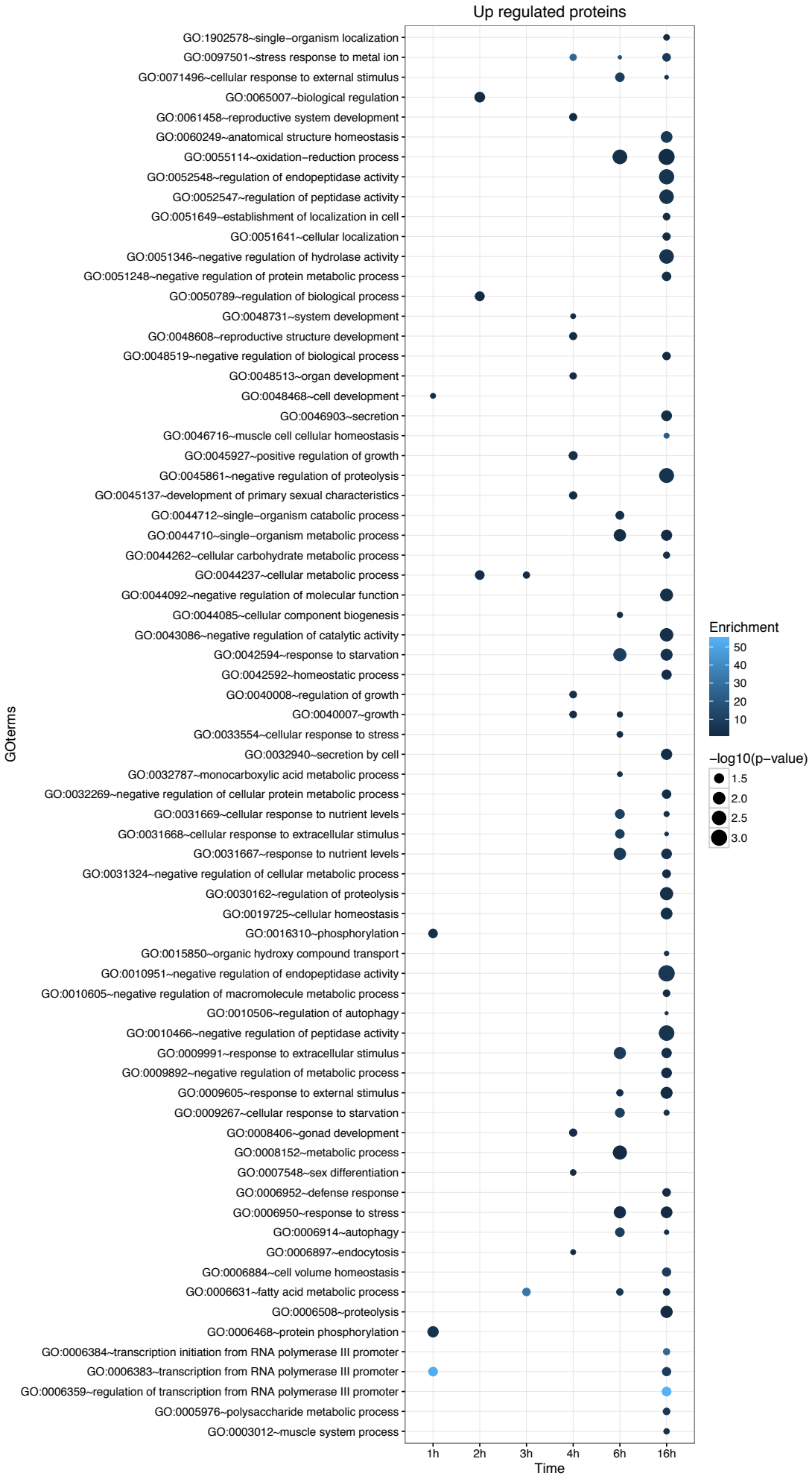
Up regulated proteins
GO:1902578~single−organism localization
GO:0097501~stress response to metal ion
GO:0071496~cellular response to external stimulus
GO:0065007~biological regulation
GO:0061458~reproductive system development
GO:0060249~anatomical structure homeostasis
GO:0055114~oxidation−reduction process
GO:0052548~regulation of endopeptidase activity
GO:0052547~regulation of peptidase activity
GO:0051649~establishment of localization in cell
GO:0051641~cellular localization
GO:0051346~negative regulation of hydrolase activity
GO:0051248~negative regulation of protein metabolic process
GO:0050789~regulation of biological process
GO:0048731~system development
GO:0048608~reproductive structure development
GO:0048519~negative regulation of biological process
GO:0048513~organ development
GO:0048468~cell development
GO:0046903~secretion
GO:0046716~muscle cell cellular homeostasis
GO:0045927~positive regulation of growth
GO:0045861~negative regulation of proteolysis
GO:0045137~development of primary sexual characteristics
GO:0044712~single−organism catabolic process
GO:0044710~single−organism metabolic process
GO:0044262~cellular carbohydrate metabolic process
GO:0044237~cellular metabolic process
GO:0044092~negative regulation of molecular function
GO:0044085~cellular component biogenesis
GO:0043086~negative regulation of catalytic activity
GO:0042594~response to starvation
GO:0042592~homeostatic process
GO:0040008~regulation of growth
GO:0040007~growth
GO:0033554~cellular response to stress
GO:0032940~secretion by cell
GO:0032787~monocarboxylic acid metabolic process
GO:0032269~negative regulation of cellular protein metabolic process
GO:0031669~cellular response to nutrient levels
GO:0031668~cellular response to extracellular stimulus
GO:0031667~response to nutrient levels
GO:0031324~negative regulation of cellular metabolic process
GO:0030162~regulation of proteolysis
GO:0019725~cellular homeostasis
GO:0016310~phosphorylation
GO:0015850~organic hydroxy compound transport
GO:0010951~negative regulation of endopeptidase activity
GO:0010605~negative regulation of macromolecule metabolic process
GO:0010506~regulation of autophagy
GO:0010466~negative regulation of peptidase activity
GO:0009991~response to extracellular stimulus
GO:0009892~negative regulation of metabolic process
GO:0009605~response to external stimulus
GO:0009267~cellular response to starvation
GO:0008406~gonad development
GO:0008152~metabolic process
GO:0007548~sex differentiation
GO:0006952~defense response
GO:0006950~response to stress
GO:0006914~autophagy
GO:0006897~endocytosis
GO:0006884~cell volume homeostasis
GO:0006631~fatty acid metabolic process
GO:0006508~proteolysis
GO:0006468~protein phosphorylation
GO:0006384~transcription initiation from RNA polymerase III promoter
GO:0006383~transcription from RNA polymerase III promoter
GO:0006359~regulation of transcription from RNA polymerase III promoter
GO:0005976~polysaccharide metabolic process
GO:0003012~muscle system process
GOterms
1h
2h
3h
4h
6h
16h
Time
Enrichment
50
40
30
20
10
−log10(p−value)
1.5
2.0
2.5
3.0

Figure S4B

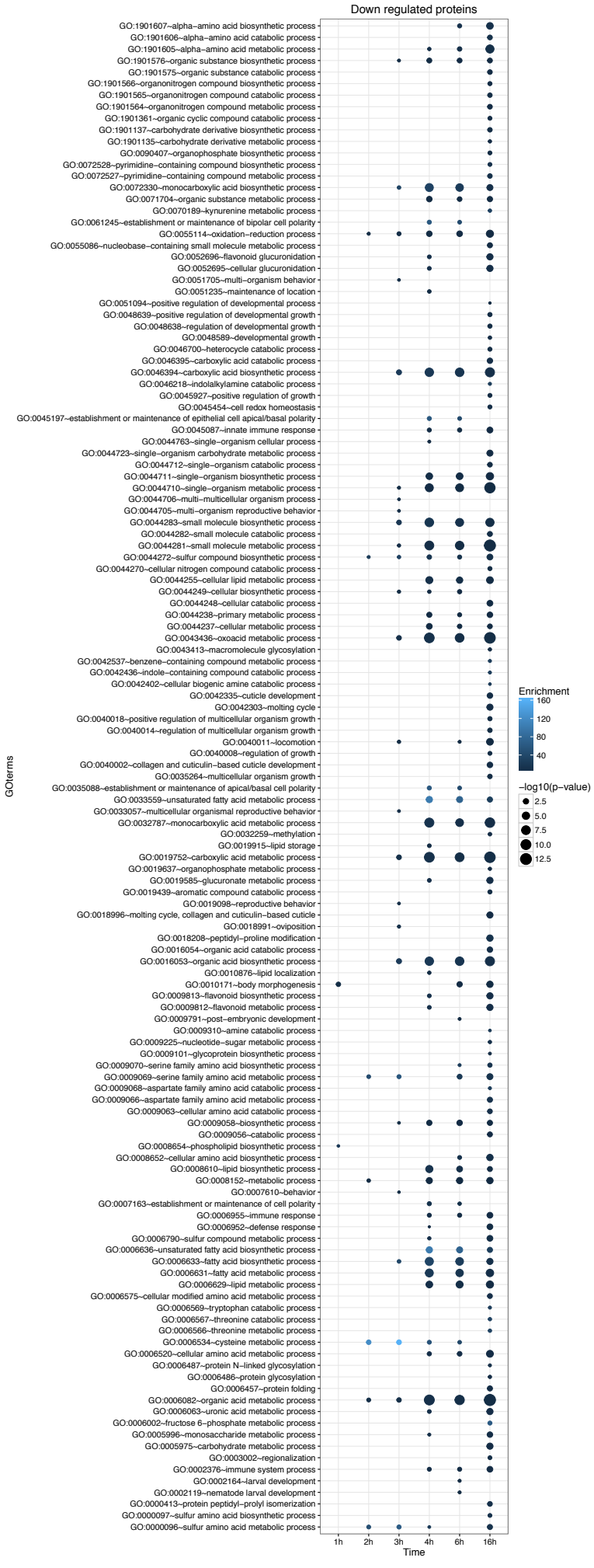
Down regulated proteins
GO:1901607~alpha~amino acid biosynthetic process
GO:1901606~alpha~amino acid catabolic process
GO:1901605~alpha~amino acid metabolic process
GO:1901576~organic substance biosynthetic process
GO:1901575~organic substance catabolic process
GO:1901566~organonitrogen compound biosynthetic process
GO:1901565~organonitrogen compound catabolic process
GO:1901564~organonitrogen compound metabolic process
GO:1901361~organic cyclic compound catabolic process
GO:1901137~carbohydrate derivative biosynthetic process
GO:1901135~carbohydrate derivative metabolic process
GO:0090407~organophosphate biosynthetic process
GO:0072528~pyrimidine~containing compound biosynthetic process
GO:0072527~pyrimidine~containing compound metabolic process
GO:0072330~monocarboxylic acid biosynthetic process
GO:0071704~organic substance metabolic process
GO:0070189~kynurenine metabolic process
GO:0061245~establishment or maintenance of bipolar cell polarity
GO:0055114~oxidation~reduction process
GO:0055086~nucleobase~containing small molecule metabolic process
GO:0052696~flavonoid glucuronidation
GO:0052695~cellular glucuronidation
GO:0051705~multi~organism behavior
GO:0051235~maintenance of location
GO:0051094~positive regulation of developmental process
GO:0048639~positive regulation of developmental growth
GO:0048638~regulation of developmental growth
GO:0048589~developmental growth
GO:0046700~heterocycle catabolic process
GO:0046395~carboxylic acid catabolic process
GO:0046394~carboxylic acid biosynthetic process
GO:0046218~indolalkylamine catabolic process
GO:0045927~positive regulation of growth
GO:0045454~cell redox homeostasis
GO:0045197~establishment or maintenance of epithelial cell apical/basal polarity
GO:0045087~innate immune response
GO:0044763~single~organism cellular process
GO:0044723~single~organism carbohydrate metabolic process
GO:0044712~single~organism catabolic process
GO:0044711~single~organism biosynthetic process
GO:0044710~single~organism metabolic process
GO:0044706~multi~multicellular organism process
GO:0044705~multi~organism reproductive behavior
GO:0044283~small molecule biosynthetic process
GO:0044282~small molecule catabolic process
GO:0044281~small molecule metabolic process
GO:0044272~sulfur compound biosynthetic process
GO:0044270~cellular nitrogen compound catabolic process
GO:0044255~cellular lipid metabolic process
GO:0044249~cellular biosynthetic process
GO:0044248~cellular catabolic process
GO:0044238~primary metabolic process
GO:0044237~cellular metabolic process
GO:0043436~oxoacid metabolic process
GO:0043413~macromolecule glycosylation
GO:0042537~benzene~containing compound metabolic process
GO:0042436~indole~containing compound catabolic process
GO:0042402~cellular biogenic amine catabolic process
GO:0042335~cuticle development
GO:0042303~molting cycle
GO:0040018~positive regulation of multicellular organism growth
GO:0040014~regulation of multicellular organism growth
GO:0040011~locomotion
GO:0040008~regulation of growth
GO:0040002~collagen and cuticulin~based cuticle development
GO:0035264~multicellular organism growth
GO:0035088~establishment or maintenance of apical/basal cell polarity
GO:0033559~unsaturated fatty acid metabolic process
GO:0033057~multicellular organismal reproductive behavior
GO:0032787~monocarboxylic acid metabolic process
GO:0032259~methylation
GO:0019915~lipid storage
GO:0019752~carboxylic acid metabolic process
GO:0019637~organophosphate metabolic process
GO:0019585~glucuronate metabolic process
GO:0019439~aromatic compound catabolic process
GO:0019098~reproductive behavior
GO:0018996~molting cycle, collagen and cuticulin~based cuticle
GO:0018991~oviposition
GO:0018208~peptidyl~proline modification
GO:0016054~organic acid catabolic process
GO:0016053~organic acid biosynthetic process
GO:0010876~lipid localization
GO:0010171~body morphogenesis
GO:0009813~flavonoid biosynthetic process
GO:0009812~flavonoid metabolic process
GO:0009791~post~embryonic development
GO:0009310~amine catabolic process
GO:0009225~nucleotide~sugar metabolic process
GO:0009101~glycoprotein biosynthetic process
GO:0009070~serine family amino acid biosynthetic process
GO:0009069~serine family amino acid metabolic process
GO:0009068~aspartate family amino acid catabolic process
GO:0009066~aspartate family amino acid metabolic process
GO:0009063~cellular amino acid catabolic process
GO:0009058~biosynthetic process
GO:0009056~catabolic process
GO:0008654~phospholipid biosynthetic process
GO:0008652~cellular amino acid biosynthetic process
GO:0008610~lipid biosynthetic process
GO:0008152~metabolic process
GO:0007610~behavior
GO:0007163~establishment or maintenance of cell polarity
GO:0006955~immune response
GO:0006952~defense response
GO:0006790~sulfur compound metabolic process
GO:0006636~unsaturated fatty acid biosynthetic process
GO:0006633~fatty acid biosynthetic process
GO:0006631~fatty acid metabolic process
GO:0006629~lipid metabolic process
GO:0006575~cellular modified amino acid metabolic process
GO:0006569~tryptophan catabolic process
GO:0006567~threonine catabolic process
GO:0006566~threonine metabolic process
GO:0006534~cysteine metabolic process
GO:0006520~cellular amino acid metabolic process
GO:0006487~protein N~linked glycosylation
GO:0006486~protein glycosylation
GO:0006457~protein folding
GO:0006082~organic acid metabolic process
GO:0006063~uronic acid metabolic process
GO:0006002~fructose 6~phosphate metabolic process
GO:0005996~monosaccharide metabolic process
GO:0005975~carbohydrate metabolic process
GO:0003002~regionalization
GO:0002376~immune system process
GO:0002164~larval development
GO:0002119~nematode larval development
GO:0000413~protein peptidyl~prolyl isomerization
GO:0000097~sulfur amino acid biosynthetic process
GO:0000096~sulfur amino acid metabolic process
GOterms
1h
2h
3h
4h
6h
16h
Time
Enrichment
160
120
80
40
−log10(p−value)
2.5
5.0
7.5
10.0
12.5

Figure S5

A

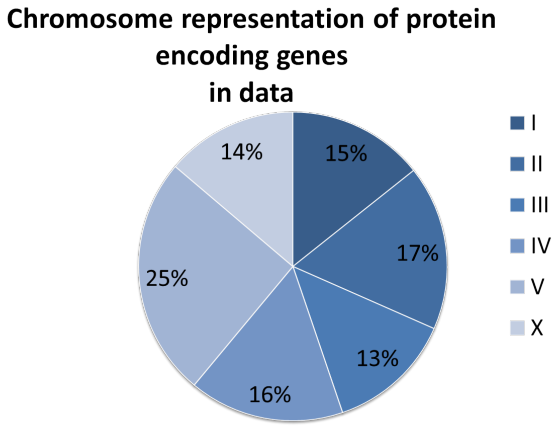
Chromosome representation of protein encoding genes in data
15%
17%
13%
16%
25%
14%
I
II
III
IV
V
X

B

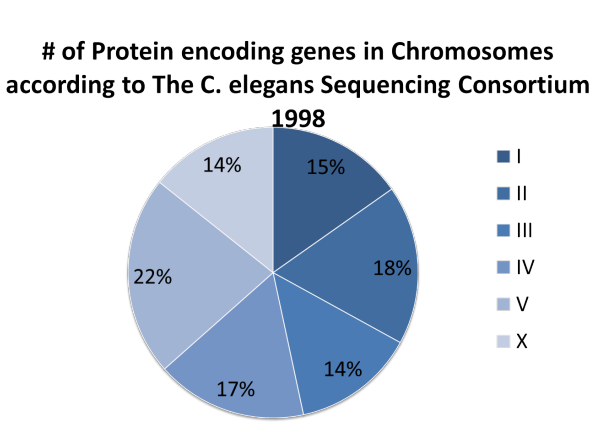
# of Protein encoding genes in Chromosomes according to The C. elegans Sequencing Consortium 1998
15%
18%
14%
17%
22%
14%
I
II
III
IV
V
X

Figure S6

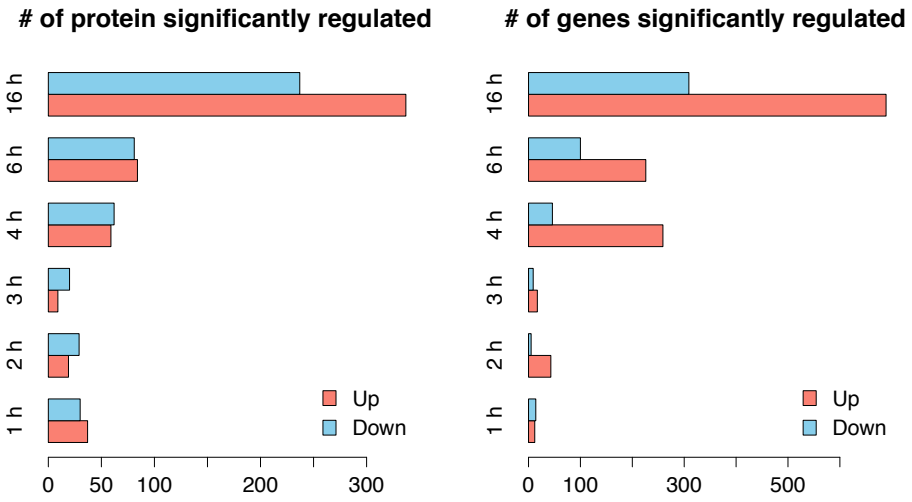
# of protein significantly regulated
16 h
6 h
4 h
3 h
2 h
1 h
Up
Down
0
50
100
200
300
# of genes significantly regulated
16 h
6 h
4 h
3 h
2 h
1 h
Up
Down
0
100
300
500

Figure S7

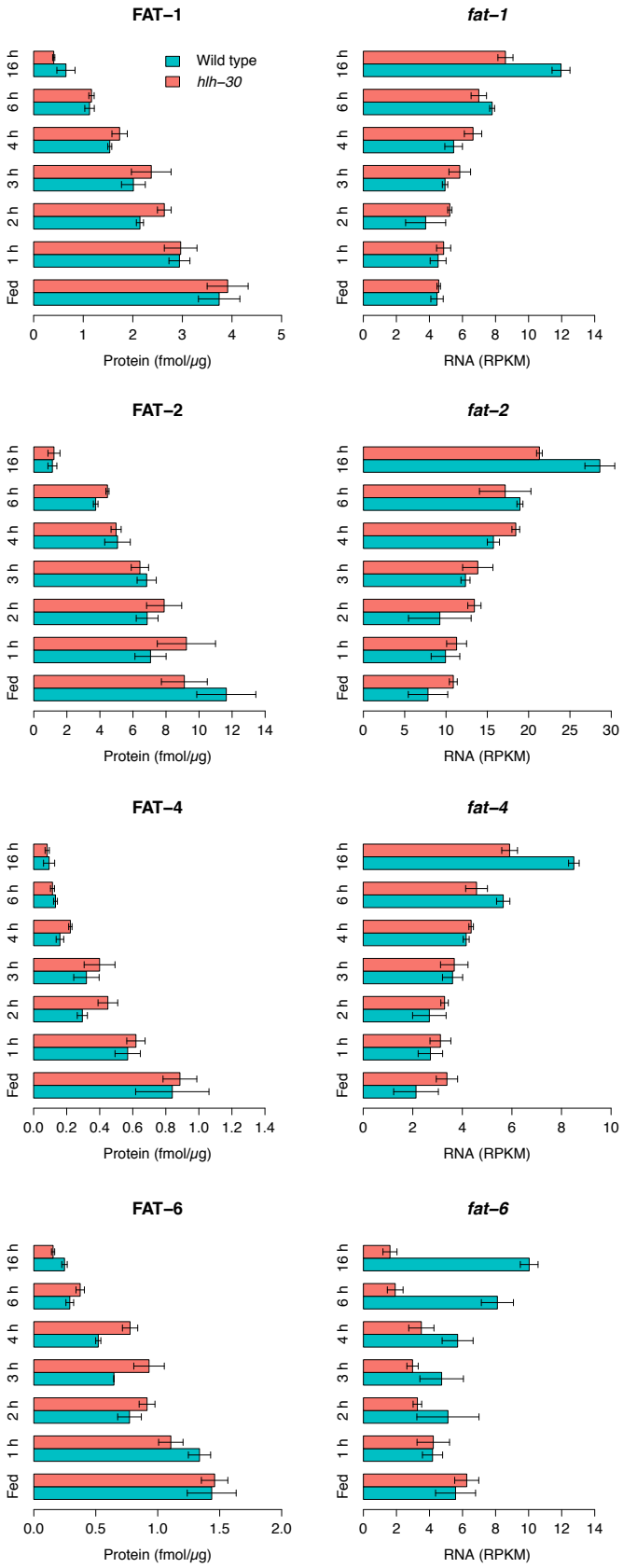
FAT–1
fat–1
FAT–2
fat–2
FAT–4
fat–4
FAT–6
fat–6
Wild type
hlh–30
16 h
6 h
4 h
3 h
2 h
1 h
Fed
Protein (fmol/μg)
RNA (RPKM)

Figure S8A


Up regulated RNA
GO:2001141~regulation of RNA biosynthetic process
GO:1903998~regulation of eating behavior
GO:1903825~organic acid transmembrane transport
GO:1903506~regulation of nucleic acid−templated transcription
GO:1902578~single−organism localization
GO:1902475~L−alpha−amino acid transmembrane transport
GO:0098900~regulation of action potential
GO:0098656~anion transmembrane transport
GO:0098542~defense response to other organism
GO:0071705~nitrogen compound transport
GO:0071495~cellular response to endogenous stimulus
GO:0071466~cellular response to xenobiotic stimulus
GO:0071407~cellular response to organic cyclic compound
GO:0071396~cellular response to lipid
GO:0071383~cellular response to steroid hormone stimulus
GO:0071310~cellular response to organic substance
GO:0070887~cellular response to chemical stimulus
GO:0060259~regulation of feeding behavior
GO:0055114~oxidation−reduction process
GO:0055085~transmembrane transport
GO:0051716~cellular response to stimulus
GO:0051707~response to other organism
GO:0051704~multi−organism process
GO:0051252~regulation of RNA metabolic process
GO:0051248~negative regulation of protein metabolic process
GO:0050896~response to stimulus
GO:0050830~defense response to Gram−positive bacterium
GO:0048583~regulation of response to stimulus
GO:0048545~response to steroid hormone
GO:0046942~carboxylic acid transport
GO:0044765~single−organism transport
GO:0044710~single−organism metabolic process
GO:0044700~single organism signaling
GO:0044281~small molecule metabolic process
GO:0044255~cellular lipid metabolic process
GO:0043401~steroid hormone mediated signaling pathway
GO:0043207~response to external biotic stimulus
GO:0043051~regulation of pharyngeal pumping
GO:0042755~eating behavior
GO:0042742~defense response to bacterium
GO:0042738~exogenous drug catabolic process
GO:0042737~drug catabolic process
GO:0042493~response to drug
GO:0042391~regulation of membrane potential
GO:0035383~thioester metabolic process
GO:0035023~regulation of Rho protein signal transduction
GO:0034654~nucleobase−containing compound biosynthetic process
GO:0034220~ion transmembrane transport
GO:0033993~response to lipid
GO:0032870~cellular response to hormone stimulus
GO:0032787~monocarboxylic acid metabolic process
GO:0032269~negative regulation of cellular protein metabolic process
GO:0031323~regulation of cellular metabolic process
GO:0023052~signaling
GO:0019438~aromatic compound biosynthetic process
GO:0019219~regulation of nucleobase−containing compound metabolic process
GO:0018130~heterocycle biosynthetic process
GO:0017144~drug metabolic process
GO:0015849~organic acid transport
GO:0015807~L−amino acid transport
GO:0015711~organic anion transport
GO:0014070~response to organic cyclic compound
GO:0010033~response to organic substance
GO:0009755~hormone−mediated signaling pathway
GO:0009725~response to hormone
GO:0009719~response to endogenous stimulus
GO:0009617~response to bacterium
GO:0009607~response to biotic stimulus
GO:0009605~response to external stimulus
GO:0009410~response to xenobiotic stimulus
GO:0008643~carbohydrate transport
GO:0007218~neuropeptide signaling pathway
GO:0007165~signal transduction
GO:0007154~cell communication
GO:0006952~defense response
GO:0006950~response to stress
GO:0006865~amino acid transport
GO:0006857~oligopeptide transport
GO:0006820~anion transport
GO:0006811~ion transport
GO:0006805~xenobiotic metabolic process
GO:0006790~sulfur compound metabolic process
GO:0006637~acyl−CoA metabolic process
GO:0006631~fatty acid metabolic process
GO:0006629~lipid metabolic process
GO:0006355~regulation of transcription, DNA−templated
GO:0006351~transcription, DNA−templated
GO:0006084~acetyl−CoA metabolic process
GO:0006082~organic acid metabolic process
GO:0003333~amino acid transmembrane transport
GO:0001508~action potential
GOterms
1h
2h
3h
4h
6h
16h
Time
−log10(p−value)
2
3
4
5
Enrichment
150
100
50

Figure S8B

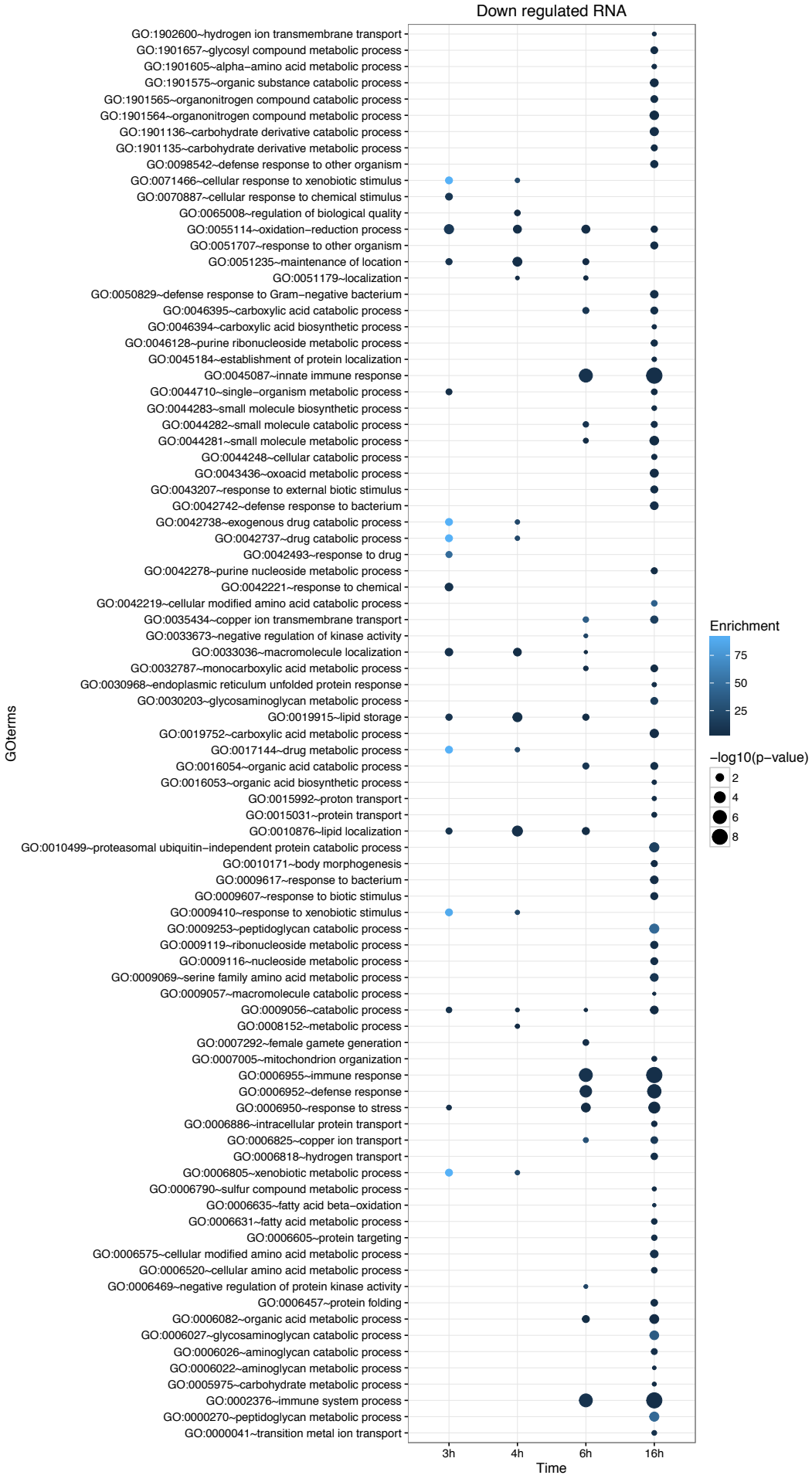
Down regulated RNA
GO:1902600~hydrogen ion transmembrane transport
GO:1901657~glycosyl compound metabolic process
GO:1901605~alpha-amino acid metabolic process
GO:1901575~organic substance catabolic process
GO:1901565~organonitrogen compound catabolic process
GO:1901564~organonitrogen compound metabolic process
GO:1901136~carbohydrate derivative catabolic process
GO:1901135~carbohydrate derivative metabolic process
GO:0098542~defense response to other organism
GO:0071466~cellular response to xenobiotic stimulus
GO:0070887~cellular response to chemical stimulus
GO:0065008~regulation of biological quality
GO:0055114~oxidation-reduction process
GO:0051707~response to other organism
GO:0051235~maintenance of location
GO:0051179~localization
GO:0050829~defense response to Gram-negative bacterium
GO:0046395~carboxylic acid catabolic process
GO:0046394~carboxylic acid biosynthetic process
GO:0046128~purine ribonucleoside metabolic process
GO:0045184~establishment of protein localization
GO:0045087~innate immune response
GO:0044710~single-organism metabolic process
GO:0044283~small molecule biosynthetic process
GO:0044282~small molecule catabolic process
GO:0044281~small molecule metabolic process
GO:0044248~cellular catabolic process
GO:0043436~oxoacid metabolic process
GO:0043207~response to external biotic stimulus
GO:0042742~defense response to bacterium
GO:0042738~exogenous drug catabolic process
GO:0042737~drug catabolic process
GO:0042493~response to drug
GO:0042278~purine nucleoside metabolic process
GO:0042221~response to chemical
GO:0042219~cellular modified amino acid catabolic process
GO:0035434~copper ion transmembrane transport
GO:0033673~negative regulation of kinase activity
GO:0033036~macromolecule localization
GO:0032787~monocarboxylic acid metabolic process
GO:0030968~endoplasmic reticulum unfolded protein response
GO:0030203~glycosaminoglycan metabolic process
GO:0019915~lipid storage
GO:0019752~carboxylic acid metabolic process
GO:0017144~drug metabolic process
GO:0016054~organic acid catabolic process
GO:0016053~organic acid biosynthetic process
GO:0015992~proton transport
GO:0015031~protein transport
GO:0010876~lipid localization
GO:0010499~proteasomal ubiquitin-independent protein catabolic process
GO:0010171~body morphogenesis
GO:0009617~response to bacterium
GO:0009607~response to biotic stimulus
GO:0009410~response to xenobiotic stimulus
GO:0009253~peptidoglycan catabolic process
GO:0009119~ribonucleoside metabolic process
GO:0009116~nucleoside metabolic process
GO:0009069~serine family amino acid metabolic process
GO:0009057~macromolecule catabolic process
GO:0009056~catabolic process
GO:0008152~metabolic process
GO:0007292~female gamete generation
GO:0007005~mitochondrion organization
GO:0006955~immune response
GO:0006952~defense response
GO:0006950~response to stress
GO:0006886~intracellular protein transport
GO:0006825~copper ion transport
GO:0006818~hydrogen transport
GO:0006805~xenobiotic metabolic process
GO:0006790~sulfur compound metabolic process
GO:0006635~fatty acid beta-oxidation
GO:0006631~fatty acid metabolic process
GO:0006605~protein targeting
GO:0006575~cellular modified amino acid metabolic process
GO:0006520~cellular amino acid metabolic process
GO:0006469~negative regulation of protein kinase activity
GO:0006457~protein folding
GO:0006082~organic acid metabolic process
GO:0006027~glycosaminoglycan catabolic process
GO:0006026~aminoglycan catabolic process
GO:0006022~aminoglycan metabolic process
GO:0005975~carbohydrate metabolic process
GO:0002376~immune system process
GO:0000270~peptidoglycan metabolic process
GO:0000041~transition metal ion transport
GOterms
3h
4h
6h
16h
Time
Enrichment
75
50
25
−log10(p−value)
2
4
6
8

Figure S9

A

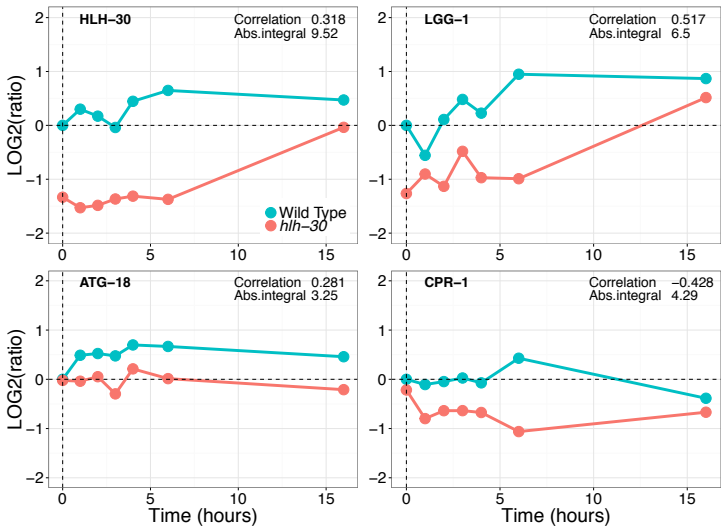
HLH−30
Correlation 0.318
Abs.integral 9.52
LGG−1
Correlation 0.517
Abs.integral 6.5
ATG−18
Correlation 0.281
Abs.integral 3.25
CPR−1
Correlation −0.428
Abs.integral 4.29
Wild Type
hlh−30
LOG2(ratio)
Time (hours)

B

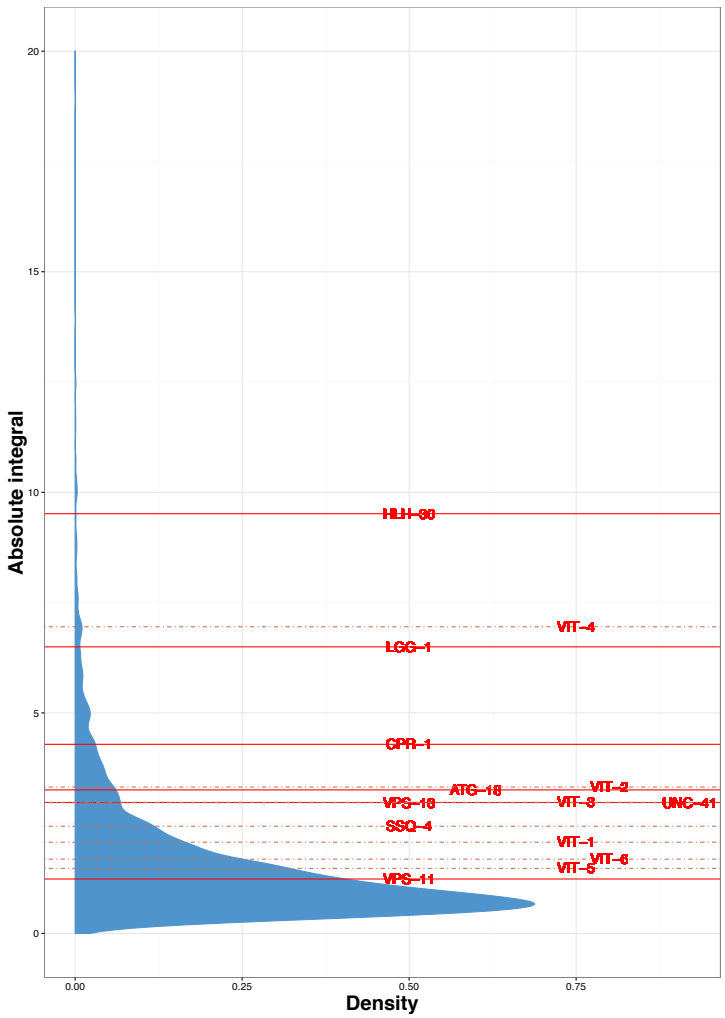
Absolute integral
Density
HLH−30
VIT−4
LGG−1
CPR−1
ATG−18
VIT−2
VPS−18
VIT−3
UNC−41
SSQ−4
VIT−1
VIT−6
VIT−5
VPS−11

Figure S10

A

	Number	Turkey's
1	0.0024	minimum
2	0.2468	lower–hinge
3	0.5215	median
4	1.0327	upper–hinge
5	21.0417	maximum

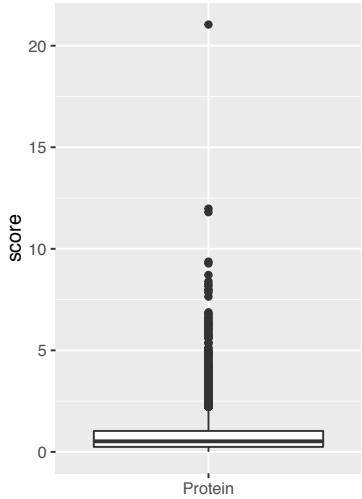

B

	Number	Turkey's
1	0.12	minimum
2	0.67	lower–hinge
3	1.07	median
4	1.85	upper–hinge
5	27.81	maximum

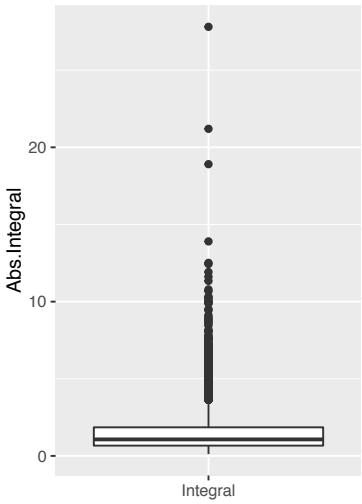

Figure S11

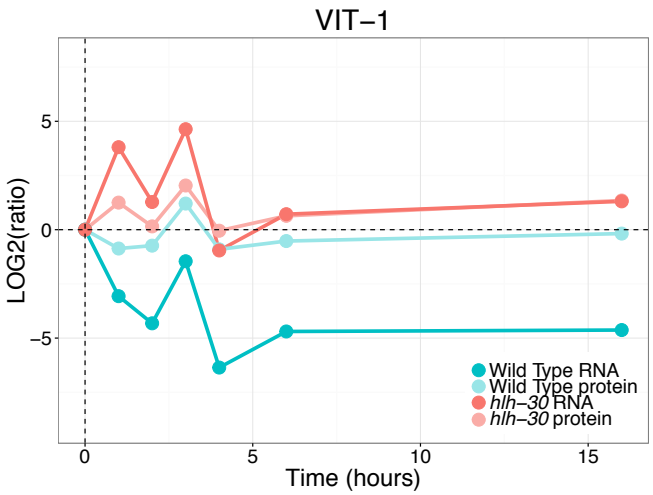
VIT−1
LOG2(ratio)
5
0
−5
0
5
10
15
Time (hours)
Wild Type RNA
Wild Type protein
hlh−30 RNA
hlh−30 protein

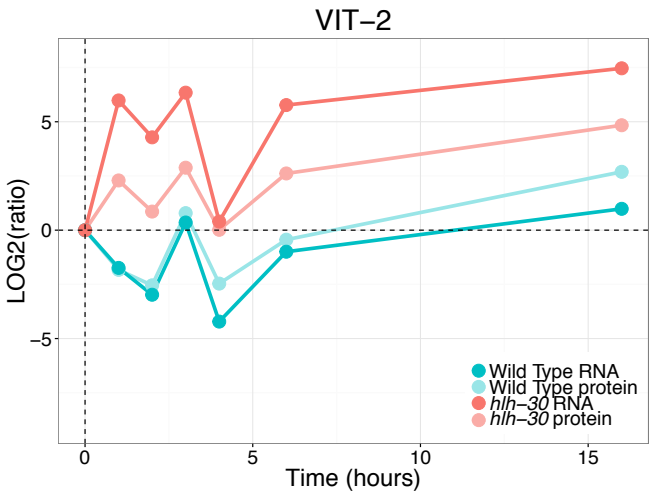
VIT−2
LOG2(ratio)
5
0
−5
0
5
10
15
Time (hours)
Wild Type RNA
Wild Type protein
hlh−30 RNA
hlh−30 protein

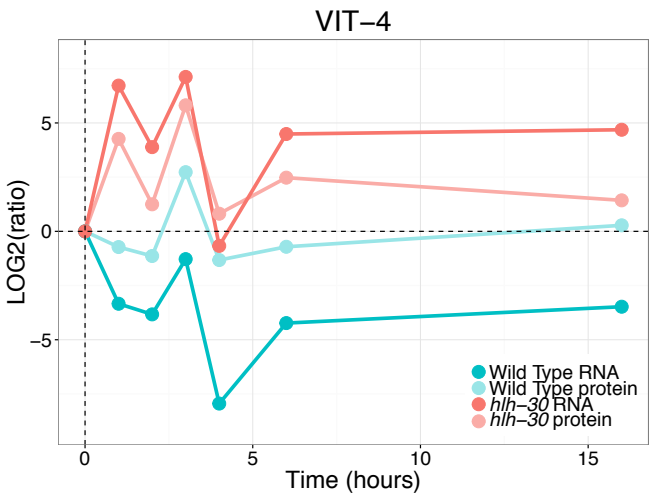
VIT−4
LOG2(ratio)
5
0
−5
0
5
10
15
Time (hours)
Wild Type RNA
Wild Type protein
hlh−30 RNA
hlh−30 protein